NASA TECHNICAL NOTE

NASA TN D-4871

VIBRATION ANALYSIS OF A 1/40-SCALE DYNAMIC MODEL OF SATURN V—LAUNCH-PLATFORM— UMBILICAL-TOWER CONFIGURATION

by Howard M. Adelman and Earl C. Steeves

Langley Research Center
Langley Station, Hampton, Va.

VIBRATION ANALYSIS OF A 1/40-SCALE DYNAMIC MODEL OF SATURN V—LAUNCH-PLATFORM—UMBILICAL-TOWER CONFIGURATION

By Howard M. Adelman and Earl C. Steeves

Langley Research Center
Langley Station, Hampton, Va.

NATIONAL AERONAUTICS AND SPACE ADMINISTRATION

VIBRATION ANALYSIS OF A 1/40-SCALE DYNAMIC MODEL OF SATURN V—

LAUNCH-PLATFORM—UMBILICAL-TOWER CONFIGURATION

By Howard M. Adelman and Earl C. Steeves
Langley Research Center

SUMMARY

An analysis was performed to determine the lateral-vibrational characteristics of a 1/40-scale dynamic model of the Apollo-Saturn V vehicle—umbilical-tower configuration. The direct stiffness method was employed for the calculations. The analysis treats the vibration of the complete configuration confined to the plane of the tower and vehicle center lines, although the tower itself was analyzed in two directions. Results are presented for the umbilical tower alone, the vehicle alone, the umbilical tower mounted on the launch platform and the complete vehicle—umbilical-tower configuration. The flexible connection between the vehicle and launch platform had to be represented by a rotational spring to obtain good agreement with experiment.

All the analytical results were compared with experimental results and the good agreement indicates that the direct stiffness method provides an effective technique for computing the vibrational characteristics of complex structures.

INTRODUCTION

Launch-vehicle systems are, in general, subjected to dynamic-loading environments such as ground winds at the launch site and launch noise at lift-off. To prevent damage to the vehicle and its supporting structures from these environments, it is necessary to have the capability of computing the dynamic response of the system to arbitrary disturbances. Often, one of the most important steps in the computation of the dynamic response is the determination of the natural frequencies and mode shapes for the system of interest.

Configurations such as the Apollo-Saturn V launch system consisting of the vehicle and its supporting structure represent very complex systems. Thus, the determination of the vibrational characteristics of this configuration requires a detailed mathematical model on which to base calculations. The methods that have previously been used to compute the vibrational characteristics of complex structures are, in general, based on replacing the structure by a series of springs and lumped masses and writing the equations of motion for the idealized structure in terms of arbitrarily assigned degrees of

freedom. The so-called finite-element method represents an improvement over previous methods in that the structure is replaced by an assemblage of structural elements such as bars, beams, and plates. These structural elements are usually coincident with the members of the actual structure and the assignment of degrees of freedom is still at the discretion of the analyst. The finite-element method is generally implemented by either of two techniques. These techniques are the force or flexibility method and the displacement or direct stiffness method.

The purpose of the analysis described herein is to demonstrate the application of the direct stiffness method to the calculation of the vibrational characteristics of a 1/40-scale dynamic model of the Apollo-Saturn V vehicle—umbilical-tower configuration. Details of the direct stiffness method are given in reference 1 and its application to vibration problems is discussed in reference 2. The analysis was carried out by using the computer program described in references 3, 4, and 5.

Natural frequencies and mode shapes were computed for five cases: the umbilical tower fixed to a rigid foundation with motion parallel to the plane of the tower and vehicle center lines, the umbilical tower mounted on the launch platform with motion in the plane of the tower and vehicle center lines, the umbilical tower fixed to a rigid foundation with motion normal to the plane of the tower and vehicle center lines, the vehicle fixed to a rigid foundation with motion parallel to the tower and vehicle center lines, and finally, the complete tower-platform-vehicle configuration (fig. 1) with motion parallel to the plane of the tower and vehicle center lines. The computed frequencies and mode shapes were compared with the experimental results of references 6 and 7. The steps in the analysis are described in detail so that the method can be directly applied to structures similar to that of the present analysis.

SYMBOLS

A   cross-sectional area, inches^2 (centimeters^2)

E   Young's modulus, pounds/inch^2 (newtons/meter^2)

f   frequency of vibration, Hertz

I   area moment of inertia, also identity matrix, inches^4 (centimeters^4)

K   element of substructure stiffness matrix

k   element of system stiffness matrix

2

l_v length of vehicle, inches (centimeters)

l_t length of umbilical tower, inches (centimeters)

M   element of substructure mass matrix

m   element of system mass matrix

P   element of reduced launch-platform stiffness matrix

R   element of rotational-spring stiffness matrix

s   system degree of freedom

T   element of reduced umbilical-tower stiffness matrix

U,V,W   matrix notation for displacement in x-, y-, and z-directions

u,v,w   displacement in x-, y-, and z-directions

X,Y,Z   axes of reference

x,y,z   longitudinal, lateral, and normal distances

β element of the coupling matrix

β_1 matrix defined by equation (12a)

β_2 matrix defined by equation (12b)

δ substructure degree of freedom

θ rotation about X-axis, radians

κ uncoupled-system stiffness matrix

μ uncoupled-system mass matrix

ϕ rotation about Y-axis, radians

ψ rotation about Z-axis, radians

ω circular frequency, radians/second

Subscripts:

a analytical

b bottom of rotational spring

e experimental

i an integer $1 \leqq i \leqq 156$

t top of rotational spring

X,Y,Z about X-, Y-, and Z-axes, respectively

Superscripts:

P launch platform

V vehicle

T umbilical tower

Matrix notation:

[ ] square or rectangular matrix

[ ]' transpose of a matrix

{ } column matrix

      Bar over symbol indicates a portion of a column matrix.

4

MODEL DESCRIPTION AND IDEALIZATION

For this analysis the 1/40-scale Saturn V—umbilical-tower configuration is considered to be composed of three substructures: the umbilical tower, the launch platform, and the Saturn V vehicle. (See fig. 1.) In this section, a brief description of each of the substructures and a discussion of how each substructure was idealized are given. Also, a brief description of the manner in which the substructures are joined and the idealization of these joining conditions are presented. The descriptions are not intended to be detailed, but are presented to indicate the reasoning behind the idealizations. A more detailed description of the model and the scaling laws which were used to relate model and full-scale properties are presented in reference 6.

Umbilical Tower

The umbilical tower is a framed structure consisting mainly of tubular-steel members. However, in the flared portion of the structure there are eight thin diagonal rod members. Groups of solid plates are located at six positions along the length of the umbilical tower. These plates are bolted at each of their corners to steel blocks which in turn are welded to the tower structure. (See fig. 1.) Some blocks are also located where there are no plates. The plates and blocks serve to assure that the 1/40-scale-model umbilical tower has a mass distribution and center of gravity that correctly represent, to model scale, the corresponding full-scale values.

For clarity, the idealized umbilical tower is shown in figure 2 in an exploded view. The plates are shown, but the blocks are omitted in this figure. The numbers on the tower faces are gridpoints or nodes, which represent the ends of various members in the idealized umbilical tower. The umbilical tower has been idealized as a three-dimensional pin-jointed structure having 376 bar members joined at 156 nodes. The plates and blocks are assumed to be rigid. To discuss the idealization of the mass distribution, the difference between corner nodes and internal nodes must be distinguished. The corner nodes are those that are located on the vertical boundaries of a face of the tower (for example, 1, 9, 17, . . .) and the internal nodes are those remaining (for example, 5, 13, 21, . . .). The mass of the umbilical tower has been lumped at the corner nodes only by first dividing the mass of every member equally between its two nodes regardless of whether it was a corner node or an internal node. Then the mass that was assigned to any internal node was divided equally among all the corner nodes to which the internal node was connected. The mass assigned to a corner node was augmented by one-fourth of the mass of any plate attached to the node plus the mass of any block located at the node.

The longitudinal vibrational frequencies of the umbilical tower were assumed to be much higher than any lateral vibrational frequencies of interest in the analysis. Therefore, the umbilical tower was represented, for longitudinal motion, as a rigid body. Since four tower-tiedown points exist, the idealization of the umbilical tower for longitudinal motion consisted of four lumped masses, each equal to one-fourth of the total tower mass.

Launch Platform

The launch platform is shown in figure 1 and details of the construction of this platform are shown in figure 3. The launch platform is basically a frame supported on 11 legs with circular cross sections. Each leg is fitted, at the lower end, into a large block, and the blocks are in turn bolted to a rigid foundation. The arrangement of the legs is not symmetrical with respect to the X-axis. (See fig. 4.) The framed portion is composed of steel I-beams with both continuous and truss-like webs. The top and bottom of the frame is covered by thin cover plates, which are welded around the periphery of the frame. Cylindrical weights are attached to several members of the frame with bolts, which penetrate the cover plate on top of the frame. The weights are included so that the model launch-platform mass distributions and center of gravity correctly represent the corresponding full-scale values. These weights are not arranged in a symmetrical manner with respect to the center line of the frame. (See fig. 1.)

The idealized launch platform is shown in figure 4. This idealization consists of a frame made of 47 beam members joined at 43 nodes and supported on 11 beam members. All the beam members have bending, stretching, torsion, and shear stiffness. The mass of the launch platform was lumped at all the nodes by first dividing the mass of each member equally between its nodes and then dividing the mass of the cover plating equally among all the nodes of the frame. Finally, the mass of each cylindrical weight was divided equally between the two nodes of the member to which the weight was attached. The amount of mass assigned to each node was equal to the sum of the contributions from these three sources.

Apollo-Saturn V Vehicle

The model of the Saturn V vehicle is shown in figure 1 and is illustrated schematically in figure 5(a). The vehicle model consists of three stages and a payload section. Each stage is composed basically of a cylindrical section, models of the engines, and weights to represent the mass of the propellants. Solid weights are included in all three stages of the model to represent the mass of fuel and liquid oxygen (LOX) in the tanks of the full-size vehicle. Containers of water were included in the second and third stages to represent the mass of liquid hydrogen (LH$_2$). The total weight represented a full-scale weight condition in which the first-stage tanks were 85 percent full and the remaining

tanks were completely full. In the first stage of the model, there are two separate spring-mass arrangements which are designed to simulate the sloshing of fuel and liquid oxygen in the respective tanks of the full-scale vehicle. The payload section consists of models of the lunar, service, and command modules and the launch-escape system.

The idealization of the model of the Saturn V vehicle is represented as a branched beam. (See fig. 5(b).) The main beam is composed of 55 beam members having bending and transverse shear stiffness, the members being joined at 56 nodes. These beam members and nodes are the same as those used in reference 7; the stiffness properties developed in this reference were used to obtain stiffness properties for a smaller number of degrees of freedom for the present analysis. The first-, second-, and third-stage engines are represented by single-degree-of-freedom branches, as are the two slosh simulators in the first stage. To reduce the number of degrees of freedom for this analysis, the mass of the vehicle is lumped at only those nodes in figure 5(b) that are represented by circles. The remaining nodes (those denoted by tick marks) are assigned zero mass. The degrees of freedom associated with the nodes having zero mass are eliminated from the equations of motion (and thus lead to a reduced-size eigenvalue problem) by a procedure described later. The mass that was lumped at a node was found by first computing the mass of each beam segment bounded by two of the nodes denoted by circles. This mass was then divided equally between these two bounding nodes. The mass of a segment of the beam included the mass of structural material in the segment plus the mass of any simulated propellant in that segment. The mass and stiffness of each branch were taken from the model specifications. The mass and stiffness properties for the main beam were taken from the model mass and EI distribution, respectively.

The Saturn V vehicle model was assumed to have longitudinal vibrational frequencies that were much higher than any lateral frequencies of interest in the present analysis. Therefore, the vehicle was idealized as a rigid body for longitudinal motion relative to the launch platform, and was represented as two lumped masses, each equal to one-half of the mass of the vehicle.

Connections Between the Substructures

The umbilical tower is bolted to the launch platform at four locations, indicated as tower tiedown points in figure 3. These locations are approximately coincident with the four nodes in figure 4 with numbers 24, 30, 32, and 37. The connection was idealized as a rigid translational connection that was expressed by equating the displacements of the tower and the displacements of the launch platform at each tower tiedown node.

The connection between the vehicle and the launch platform is effected by bolting four vehicle-attachment blocks to the vehicle at its lower end and then by bolting each of these attachment blocks to a corresponding vehicle-support block which is welded to

the launch platform. The locations of the vehicle-support blocks on the launch platform are denoted as vehicle tiedown points in figure 3. The connection of the vehicle to the launch platform was idealized by a rigid translational connection and a flexible rotational connection; that is, the displacements of the vehicle were set equal to the displacements of the launch-platform tiedown nodes (nodes 3 and 4 in fig. 4) but the rotation of the vehicle at the tiedown node was set equal to the rotation of one side of a rotational spring and the rotation of the launch platform at each tiedown node was set equal to the rotation of the other side of the spring. This spring simulates the local flexibility of the vehicle tiedown structure, which is not included in the elastic representation of either the launch platform or vehicle. The spring rate for this idealization was determined empirically. This method of representing the connection was suggested in reference 7 where it was found that assuming a rigid rotational connection (that is, equating the rotations) led to lateral frequencies of the vehicle which were higher than the corresponding experimental frequencies. However, by assuming a flexible rotational connection, the analytical frequencies were made to agree with the experimental frequencies. The flexible rotational connection is shown schematically in sketch 1. (The arrows indicate positive direction.)

Sketch 1
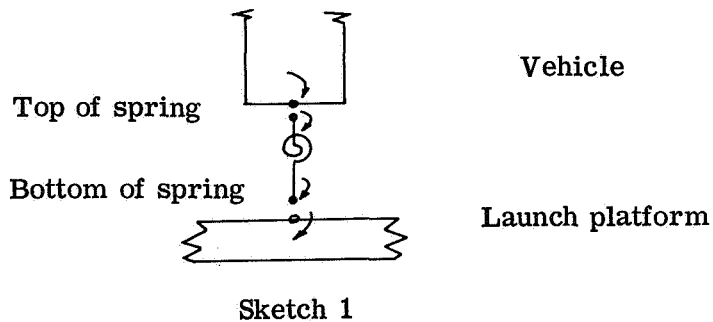
ANALYSIS

Method of Analysis

The analysis was performed by using the direct stiffness method as implemented by the computer program of references 3 to 5. Briefly, the steps in the analysis were as follows: stiffness and mass matrices for each of the three substructures (the umbilical tower, the launch platform, and the Saturn V vehicle) were developed in terms of the degrees of freedom of the substructures. Next, a transformation matrix was introduced which related the degrees of freedom of each substructure to the degrees of freedom of the system. By using this transformation matrix, the substructure stiffness and mass matrices were combined to form system stiffness and mass matrices. With these matrices, the equations of free vibration of the system were written and transformed to a classical eigenvalue problem which was solved by the method of Jacobi.

8

Development of Substructure Stiffness Matrices

The stiffness matrix for each substructure was generated in terms of all the elastic degrees of freedom of the substructure. To keep the size of the final eigenvalue problem within the capacity of the computer program used, certain degrees of freedom were constrained to be zero, whereas others were removed as explicit variables by associating zero inertia with them. These two operations resulted in the substructure stiffness matrices that were used in the remainder of the analysis. In this section, the method of obtaining these substructure matrices is described.

Umbilical-tower stiffness matrix.- Information describing the structural properties and geometry of the umbilical tower was read into the computer program of references 3 to 5. This information consisted of the elastic constants and the area of each member of the idealized umbilical tower as well as the coordinates of each node with respect to the Cartesian references axes, X, Y, and Z (fig. 2). The areas and coordinates are presented in tables I and II, respectively. The tower material was steel, and the value of Young's modulus used was 30×10^6 psi (2.068×10^{12} N/m^2). On the basis of this input, stiffness matrices were generated for each member of the idealized umbilical tower. (See ref. 3, pp. 44-47 for the form of these matrices.) The matrices were then superimposed to yield the complete umbilical-tower stiffness matrix. This matrix with its associated degrees of freedom is represented symbolically as follows:

$$
[K]\{\delta\} =
\begin{bmatrix}
K_{11} & K_{12} & & & & & K_{17} & K_{18} & K_{19} \\
K_{21} & & & & & & \cdot & \cdot & \cdot \\
\cdot & & & & & & & & \\
& & & & & & \cdot & \cdot & \cdot \\
\cdot & & & & & & & & \\
& & & & & & \cdot & \cdot & \cdot \\
K_{71} & \cdot & \cdot & \cdot & & & K_{77} & K_{78} & \\
K_{81} & \cdot & \cdot & \cdot & & & K_{87} & K_{88} & \\
K_{91} & \cdot & \cdot & \cdot & & & & & K_{99}
\end{bmatrix}
\begin{Bmatrix}
\bar{U}_1^T \\
\bar{U}_2^T \\
\bar{U}_3^T \\
\bar{U}_4^T \\
\bar{U}_5^T \\
\bar{U}_6^T \\
\bar{U}_7^T \\
\bar{W}^T \\
\bar{V}^T
\end{Bmatrix}
\tag{1}
$$

The vectors $\bar{U}_1^T$ to $\bar{V}^T$ and the coordinate system for the umbilical tower are defined in figure 2. The elements of the matrix (eq. (1)) are themselves matrices.

For most of the configurations analyzed, the motion of the umbilical tower was restricted to be parallel to the plane of the vehicle and tower center lines. The displacements normal to this plane (the V-displacements) are therefore eliminated completely by deleting from the stiffness matrix the rows and columns associated with the V-displacements (represented in eq. (1) by row 9 and column 9).

Next, the W-displacements at all the nodes and the U-displacements at the internal nodes are eliminated from the problem as explicit variables under the provision that zero inertia is associated with these displacements. This elimination followed the method of reference 2 (p. 44) and resulted in a reduced stiffness matrix for the umbilical tower:

$$
\begin{bmatrix} T_{11} & T_{12} & \cdot & \cdot & \cdot & T_{16} \\ T_{21} & \cdot & & & & \\ \cdot & & & & & \\ \cdot & & & & \cdot & \\ \cdot & & & \cdot & & \\ T_{61} & & & & & T_{66} \end{bmatrix} = \begin{bmatrix} K_{11} & K_{12} & \cdot & \cdot & \cdot & K_{16} \\ K_{21} & \cdot & & & & \cdot \\ \cdot & & & & & \cdot \\ \cdot & & & & & \cdot \\ \cdot & & & & & \cdot \\ K_{61} & & & & & K_{66} \end{bmatrix} - \begin{bmatrix} K_{17} & K_{18} \\ \cdot & \cdot \\ \cdot & \cdot \\ \cdot & \cdot \\ K_{67} & K_{68} \end{bmatrix} \begin{bmatrix} K_{77} & K_{78} \\ K_{87} & K_{88} \end{bmatrix}^{-1} \begin{bmatrix} K_{71} & \cdot & \cdot & \cdot & K_{76} \\ K_{81} & \cdot & \cdot & \cdot & K_{86} \end{bmatrix} \quad (2)
$$

where, in equation (2), T represents an element of the reduced stiffness matrix for the umbilical tower and K represents an element of the original umbilical-tower stiffness matrix (eq. (1)). The reduced stiffness matrix for the umbilical tower is expressed in terms of the U-displacements of the 76 corner nodes of the umbilical tower. This stiffness matrix is combined with the other substructure matrices to form the system stiffness matrix.

Launch-platform stiffness matrix.- Information describing the structural properties and geometry of the launch platform was read into the computer program of references 3 to 5. This information consisted of the elastic constants for the material of the launch platform, the section properties for each member, and the coordinates of each node of the launch platform. The material used was steel with a Young's modulus of 30×10^6 psi $(2.068 \times 10^{12}$ N/m$^2)$ and a Poisson's ratio of 0.30. The section properties and coordinates are presented in tables III and IV, respectively. The effective shear areas in the X- and Y-directions were taken to be one-half the actual cross-sectional area. On the basis of the input, a stiffness matrix was generated by the computer program for each

10

member of the launch platform. Then by superposition, the complete stiffness matrix for the launch platform was obtained. This matrix, with its associated degrees of freedom, is represented symbolically as follows:

$$
[K]\{\delta\} =
\begin{bmatrix}
K_{1,1} & K_{1,2} & K_{1,3} & K_{1,4} & K_{1,5} & K_{1,6} & K_{1,7} & K_{1,8} & K_{1,9} & K_{1,10} & K_{1,11} & K_{1,12} & K_{1,13} \\
K_{2,1} & & & & & & & & & & & & \\
K_{3,1} & & & & & & & & & & & & \\
K_{4,1} & & & & & & & & & & & & \\
K_{5,1} & & & & & & & & & & & & \\
K_{6,1} & & & & & & & & & & & & \\
K_{7,1} & & & & & & & & & & & & \\
K_{8,1} & & & & & & & & & & & & \\
K_{9,1} & & & & & & & & & & & & \\
K_{10,1} & & & & & & & & & & & & \\
K_{11,1} & & & & & & & & & & & & \\
K_{12,1} & & & & & & & & & & & & \\
K_{13,1} & & & & & & & & & & & & K_{13,13}
\end{bmatrix}
\begin{Bmatrix}
\overline{w}_1^P \\
\overline{w}_2^P \\
\overline{w}_3^P \\
\overline{u}_1^P \\
\overline{\phi}_1^P \\
\overline{\phi}_2^P \\
\overline{\theta}_1^P \\
\overline{v}^P \\
\overline{\psi}^P \\
\overline{u}_2^P \\
\overline{w}_4^P \\
\overline{\phi}_3^P \\
\overline{\theta}_2^P
\end{Bmatrix}
\qquad (3)
$$

Here the elements of the launch-platform matrix are themselves matrices. The vectors $\overline{w}_1^P$ to $\overline{\theta}_2^P$ are defined in figure 4 along with the coordinate system of the launch platform. To obtain the hold-down condition of the launch platform, all three displacements and all three rotations at the hold-down nodes (nodes 19, 20, 23, 27, 29, 34, 35, 40, 41, 42, and 43) (the bottom end of each leg) were set equal to zero. Thus, the respective rows and columns associated with these displacements were deleted from the stiffness matrix. Also, to constrain the motion of the platform in a direction parallel to the x-direction, the v-displacements and ψ-rotations at all the nodes were set equal to zero; again, the corresponding rows and columns were deleted from the stiffness matrix. By this method the rows and columns of the launch-vehicle stiffness matrix which are represented in equation (3) by rows and columns 8 to 13 were deleted. The next step was to eliminate, as explicit variables, the ϕ-rotations at all nodes except the two vehicle tie-down nodes (nodes 3 and 4), thus $\overline{\phi}_2^P$ was eliminated. The θ-rotations at all nodes were eliminated as explicit variables. These two eliminations were based on the assignment of zero inertia to the rotations in question. The reduced stiffness matrix for the launch platform was then obtained by following the method of reference 2 (p. 44) as:

$$
\begin{bmatrix} P_{11} & P_{12} & \cdot & \cdot & \cdot & P_{15} \\ P_{21} & \cdot & & & & \\ \cdot & & & & & \\ \cdot & & & & & \\ \cdot & & & & \cdot & \\ P_{51} & & & & & P_{55} \end{bmatrix} = \begin{bmatrix} K_{11} & K_{12} & \cdot & \cdot & \cdot & K_{15} \\ K_{21} & \cdot & & & & \\ \cdot & & & & & \\ \cdot & & & & & \\ \cdot & & & & \cdot & \\ K_{51} & & & & & K_{55} \end{bmatrix} - \begin{bmatrix} K_{16} & K_{17} \\ K_{26} & K_{27} \\ \cdot & \cdot \\ \cdot & \cdot \\ \cdot & \cdot \\ K_{56} & K_{57} \end{bmatrix} \begin{bmatrix} K_{66} & K_{67} \\ K_{76} & K_{77} \end{bmatrix}^{-1} \begin{bmatrix} K_{61} & \cdot & \cdot & \cdot & K_{65} \\ K_{71} & \cdot & \cdot & \cdot & K_{75} \end{bmatrix} \tag{4}
$$

where P represents an element (still a matrix) of the reduced launch-platform stiffness matrix and K represents an element of the original launch-platform stiffness matrix. The reduced launch-platform stiffness matrix is expressed in terms of the w-displacements at 32 nodes, the u-displacements at 32 nodes, and the ϕ-rotations at 2 nodes. The platform stiffness matrix (eq. (4)) is subsequently combined with the other substructure stiffness matrices to form the system stiffness matrix.

Saturn V vehicle stiffness matrix.- The stiffness matrix for the model of the Saturn V vehicle was obtained by rewriting the element transfer matrices of reference 7 as element stiffness matrices and by combining these element stiffness matrices by superposition. The complete vehicle stiffness matrix with its associated degrees of freedom is shown symbolically as:

$$
[K] \{\delta\} = \begin{bmatrix} K_{11} & & & & K_{15} \\ \cdot & & & & \cdot \\ \cdot & & & & \cdot \\ \cdot & & & \cdot & \cdot \\ K_{51} & & & & K_{55} \end{bmatrix} \begin{Bmatrix} \bar{U}_1^V \\ \bar{U}_2^V \\ \bar{\phi}_1^V \\ \bar{\phi}_2^V \\ \bar{U}_3^V \end{Bmatrix} \tag{5}
$$

where the vectors $\bar{U}_1^V$ to $\bar{U}_3^V$ are defined in figure 5. This stiffness matrix is reduced by assuming that zero inertia is assigned to the rotations and that the translatory inertia is lumped only at the selected nodes (appearing in fig. 5(b) as circles). In accordance with the lumping procedure described under "Model Description and Idealization," mass was assigned only to those degrees of freedom in figure 5(b) which are denoted as $\bar{U}_1^V$ and $\bar{U}_2^V$ (symbolized by circles). The degrees of freedom to be eliminated

as explicit variables, $\bar{U}_3^V$ and $\bar{\phi}_2^V$, are assigned zero inertia. Then, according to reference 2 (p. 44), the reduced vehicle stiffness matrix is given by:

$$
\begin{bmatrix} V_{11} & V_{12} & V_{13} \\ V_{21} & V_{22} & V_{23} \\ V_{31} & V_{32} & V_{33} \end{bmatrix} = \begin{bmatrix} K_{11} & K_{12} & K_{13} \\ K_{21} & K_{22} & K_{23} \\ K_{31} & K_{32} & K_{33} \end{bmatrix} - \begin{bmatrix} K_{14} & K_{15} \\ K_{24} & K_{25} \\ K_{34} & K_{35} \end{bmatrix} \begin{bmatrix} K_{44} & K_{45} \\ K_{54} & K_{55} \end{bmatrix}^{-1} \begin{bmatrix} K_{41} & K_{42} & K_{43} \\ K_{51} & K_{52} & K_{53} \end{bmatrix} \qquad (6)
$$

The reduced vehicle stiffness matrix is expressed in terms of the u-displacements at 25 nodes and a ϕ-rotation at the vehicle-tiedown point. By using the bending and shear stiffness of the vehicle presented in reference 7, the idealization shown in figure 5, and the calculation steps just outlined, the reduced vehicle stiffness matrix was obtained. The reduced vehicle matrix is presented in table V.

The stiffness matrix representing the rotational spring at the vehicle tiedown node along with its associated rotations is

$$
\begin{bmatrix} K \end{bmatrix} \left\{ \phi \right\} = \begin{bmatrix} R & -R \\ -R & R \end{bmatrix} \left\{ \begin{array}{c} \phi_t \\ \phi_b \end{array} \right\} \qquad (7)
$$

The determination of R is discussed subsequently.

Development of substructure mass matrices.- A diagonal mass matrix for each of the substructures was obtained by first lumping the mass of the substructure at certain nodes of the substructure as described under "Model Description and Idealization." The mass was then assigned in such a manner that inertia loads were applied only in specified directions. For example, the mass of the umbilical tower was effective only in the direction parallel to the plane through the tower and vehicle center lines (that is, the x-direction). The mass of the launch platform was effective in the z-direction and in the x-direction. Finally, the mass of the vehicle was effective only in the x-direction. The mass at a certain node and acting in a given direction was placed in the mass matrix array in a location corresponding to its degree of freedom. When this placement was made for every node having mass and for every allowable direction at that node, the substructure mass matrix was obtained. The mass matrix for the launch platform was augmented by adding one-fourth of the total umbilical-tower mass to the mass assigned to

the displacements represented by $\bar{W}_2^P$ and by adding one-half of the vehicle mass to

the displacements represented by $\bar{W}_3^P$. These masses represent the effect of the

rigid-body longitudinal motion of the umbilical tower and the vehicle, respectively. The mass matrices are represented symbolically with their associated degrees of freedom as follows:

For the umbilical tower:

$$
[M]\{\delta\} = \begin{bmatrix} M_1^T & & & & & \\ & M_2^T & & & & \\ & & & & & \\ & & & & & \\ & & & & & \\ & & & & & M_6^T \end{bmatrix} \begin{Bmatrix} \bar{U}_1^T \\ \bar{U}_2^T \\ \bar{U}_3^T \\ \bar{U}_4^T \\ \bar{U}_5^T \\ \bar{U}_6^T \end{Bmatrix} \tag{8a}
$$

For the launch platform:

$$
[M]\{\delta\} = \begin{bmatrix} M_1^P & & \\ & M_2^P & \\ & & 0 \end{bmatrix} \begin{Bmatrix} \bar{W}^P \\ \bar{U}^P \\ \bar{\phi}_1^P \end{Bmatrix} \tag{8b}
$$

where for simplicity, all the w-displacements of the launch platform are written together as a single vector $\bar{W}^P$.

For the vehicle:

$$
[M]\{\delta\} = \begin{bmatrix} M_1^V & & \\ & M_2^V & \\ & & 0 \end{bmatrix} \begin{Bmatrix} \bar{U}_1^V \\ \bar{U}_2^V \\ \bar{\phi}_1^V \end{Bmatrix} \tag{8c}
$$

The actual masses appearing in the substructure mass matrices are presented in tables VI, VII, and VIII.

14

Synthesis of System Stiffness and Mass Matrices

The idealization of the complete configuration is shown in figure 6. In this figure the three idealized substructures are shown joined together and the system degrees of freedom are defined. To form the stiffness and mass matrices for the system, a transformation of the degrees of freedom was introduced. This transformation has the form

$$\{\delta\} = [\beta] \{s\} \tag{9}$$

where

$\{\delta\}$ vector of substructure degrees of freedom

$\{s\}$ vector of system degrees of freedom

$[\beta]$ relation between two vectors

For the present analysis, the elements of β are either unity or zero. On the basis of the relationship expressed by equation (9), the system stiffness and mass matrices may be obtained (see ref. 2, pp. 43 and 73):

$$[k] = [\beta]' [\kappa] [\beta] \tag{10}$$

$$[m] = [\beta]' [\mu] [\beta] \tag{11}$$

where the prime denotes a transposed matrix. For the present problem, equation (9) has the following form:

$$
\left\{
\begin{array}{c}
\bar{U}_1^T \\
\bar{U}_2^T \\
\bar{U}_3^T \\
\bar{U}_4^T \\
\bar{U}_5^T \\
\bar{U}_6^T \\
W^P \\
\bar{U}_1^P \\
\bar{\phi}_1^P \\
\bar{\phi}_b \\
\bar{\phi}_t \\
\bar{U}_1^V \\
\bar{U}_2^V \\
\bar{\phi}_1^V
\end{array}
\right\}
=
\left\{
\begin{array}{ccccccc}
I & & & & & & \\
& I & & & & & \\
& I & & & & & \\
& I & & & & & \\
& I & & & & & \\
& & \beta_1 & & & & \\
& & & I & & & \\
& & \beta_2 & & & & \\
& & & & 1 & & \\
& & & & 1 & & \\
& & & & & 1 & \\
& & & & & & I \\
& & 1 & & & & \\
& & & & & 1 &
\end{array}
\right\}
\left\{
\begin{array}{c}
\bar{s}_1 \\
\bar{s}_2 \\
\bar{s}_3 \\
\bar{s}_4 \\
\bar{s}_5 \\
\bar{s}_6 \\
\bar{s}_7
\end{array}
\right\}
\tag{12a}
$$

where $\bar{s}_1$ to $\bar{s}_7$ are defined in figure 6 and

$$
\left[\beta_1\right] = \begin{bmatrix} 1 \\ 1 \\ 1 \\ 1 \end{bmatrix}_{4 \times 1}
\tag{12b}
$$

16

$$[\beta_2] = \begin{bmatrix} 1 \\ 1 \\ \cdot \\ \cdot \\ \cdot \\ 1 \end{bmatrix}_{32 \times 1} \tag{12c}$$

Equations (12) expresses three types of relationships: Joining conditions are expressed by equating displacements or rotations of adjacent substructures at their point of connection; any equalities between displacements of nodes on the same substructure are expressed, and substructure degrees of freedom are renamed as system degrees of freedom. To explain the meaning of equations (12) further, it is expanded.

$$\left\{ U_1^T \right\} = \left\{ s_1 \right\} \tag{13}$$

$$\left\{ U_2^T \right\} = \left\{ U_3^T \right\} = \left\{ U_4^T \right\} = \left\{ U_5^T \right\} = \left\{ s_2 \right\} \tag{14}$$

$$\left\{ U_6^T \right\} = \left[\beta_1 \right] s_3 \tag{15}$$

$$\left\{ w^P \right\} = \left\{ s_4 \right\} \tag{16}$$

$$\left\{ U_1^P \right\} = \left[\beta_2 \right] s_3 \tag{17}$$

$$\left\{ \phi_1^P \right\} = \phi_b = s_5 \tag{18}$$

$$\left\{ U_1^V \right\} = \left\{ s_7 \right\} \tag{19}$$

$$U_2^V = s_3 \tag{20}$$

$$\phi_1^V = \phi_t = s_6 \tag{21}$$

Equations (13), (16), and (19) simply rename those degrees of freedom of the tower, launch platform, and vehicle for which no constraints are stated. Equation (14) expresses the condition that all nodes of the umbilical tower joined by a common plate have the same u-displacement. Equation (15) expresses the joining condition between the umbilical tower and launch platform, and equation (17) expresses the condition that all the nodes on the frame of the launch platform have the same u-displacement. Equation (18) equates the rotation of the launch platform at the vehicle tiedown node to the rotation of the bottom of the rotational spring. Equation (20), along with equation (17), expresses the joining condition between the vehicle and launch platform. Equation (21) equates the rotation of the vehicle at the vehicle tiedown node to the rotation for the top of the rotational spring. The implication of equation (17) is that the degree of freedom represented in figure 6 as s_3 is a rigid-body "swaying" of the system on the legs of the launch platform.

The matrices $\begin{bmatrix} K \end{bmatrix}$ and $\begin{bmatrix} \mu \end{bmatrix}$ along with their associated degrees of freedom have the following form:

$$
[K]\{\delta\} =
\left[
\begin{array}{cccc:ccc:cc:ccc}
T_{11} & T_{12} & \cdots & T_{16} & & 0 & & 0 & & & 0 & \\
T_{21} & & & & & & & & & & & \\
\cdot & & & & & & & & & & & \\
\cdot & & & \cdot & & & & & & & & \\
\cdot & & & & & & & & & & & \\
T_{61} & & & T_{66} & & & & & & & & \\
\hdashline
 & & & & P_{11} & P_{12} & P_{13} & & & & & \\
 & 0 & & & P_{21} & P_{22} & P_{23} & & 0 & & 0 & \\
 & & & & P_{31} & P_{32} & P_{33} & & & & & \\
\hdashline
 & 0 & & & & 0 & & R & -R & & 0 & \\
 & & & & & & & -R & R & & & \\
\hdashline
 & & & & & & & & & V_{11} & V_{12} & V_{13} \\
 & 0 & & & & 0 & & & 0 & V_{21} & V_{22} & V_{23} \\
 & & & & & & & & & V_{31} & V_{32} & V_{33} \\
\end{array}
\right]
\left\{
\begin{array}{c}
\bar{u}_1^T \\
\bar{u}_2^T \\
\bar{u}_3^T \\
\bar{u}_4^T \\
\bar{u}_5^T \\
\bar{u}_6^T \\
w^P \\
\bar{u}_1^P \\
\bar{\phi}_1^P \\
\bar{\phi}_b \\
\bar{\phi}_t \\
\bar{u}_1^V \\
\bar{u}_2^V \\
\phi_1^V \\
\end{array}
\right\}
\qquad (22)
$$

18

$$[\mu]\{\bar{\delta}\} = \begin{bmatrix} M_1^T & & & & & & & & & & & & & 0 \\ & M_2^T & & & & & & & & & & & & \\ & & M_3^T & & & & & & & & & & & \\ & & & M_4^T & & & & & & & & & & \\ & & & & M_5^T & & & & & & & & & \\ & & & & & M_5^T & & & & & & & & \\ & & & & & & M_1^P & & & & & & & \\ & & & & & & & M_2^P & & & & & & \\ & & & & & & & & 0 & & & & & \\ & & & & & & & & & 0 & & & & \\ & & & & & & & & & & 0 & & & \\ & & & & & & & & & & & M_1^V & & \\ & & & & & & & & & & & & M_2^V & \\ 0 & & & & & & & & & & & & & 0 \end{bmatrix} \begin{Bmatrix} \bar{u}_1^T \\ \bar{u}_2^T \\ \bar{u}_3^T \\ \bar{u}_4^T \\ \bar{u}_5^T \\ \bar{u}_6^T \\ \bar{w}^P \\ \bar{u}_1^P \\ \bar{\phi}_1^P \\ \bar{\phi}_b \\ \bar{\phi}_t \\ \bar{u}_1^V \\ \bar{u}_2^V \\ \bar{\phi}_1^V \end{Bmatrix} \tag{23}$$

In equation (23) the mass matrices are written in terms of submatrices for clarity.

Determination of Frequencies and Mode Shapes

The operations of equations (10) and (11) yield the system stiffness and mass matrices. The equations of free vibration of the system are then expressible as

$$[k]\{s\} = \omega^2 [m]\{s\} \tag{24}$$

where k, m, and s have been previously defined and ω is the undetermined natural frequency of the system. The mass matrix is singular because zero inertia is associated with the rotation of the system at the vehicle tiedown node. This condition presents no problem, however, since the mass matrix does not have to be inverted. Equation (24) is transformed to a standard eigenvalue problem by performing a Choleski decomposition of the mass matrix as described in reference 5 (pp. 104-107). The resulting eigenvalue problem is solved by using the method of Jacobi to yield the frequencies and mode shapes of the idealized system. In addition to computing the frequencies and mode shapes of the complete configuration, it was also desired to compute the frequencies and mode shapes of the umbilical tower alone in the x- and y-directions fixed to a rigid foundation, the tower and platform together, and the vehicle alone fixed to a rigid foundation. The steps

leading to the computations for the configurations previously mentioned are simply special cases of the steps outlined previously. Each of the equations to be solved have the same form as equation (24) but equations (22) and (23) contain only the stiffness and mass matrices of the substructure(s) involved in the configuration under consideration. Also, the β-matrix contains only those rows and columns corresponding to the substructure(s) of the configuration involved. In addition, for the umbilical tower, the rows and columns of the stiffness, mass, and β-matrices corresponding to the u-displacements of the tower tiedown points were deleted. Thus equation (15) is replaced by the equation $U_6^T = 0$. The analysis of the tower in the y-direction was accomplished by interchanging the roles of the u- and v-displacements in the steps outlined.

For the vehicle alone, the rows and columns corresponding to the u-displacement at the vehicle tiedown points and the rows and columns corresponding to the rotation of the bottom of the rotational spring were deleted from the stiffness, mass, and β-matrices. Thus equations (18) and (20) are replaced by the equations $\phi_b = 0$ and $U_2^V = 0$, respectively.

Finally, for the umbilical tower and launch platform, the mass matrix for the launch platform did not have to be augmented by the mass of the vehicle at the vehicle tiedown points because the vehicle was not included in this configuration.

RESULTS AND DISCUSSION

The results of the analysis are presented in terms of resonant frequencies and mode shapes of each of the four configurations studied. These results appear in table IX and in figures 7 to 10 along with experimental results from references 6 and 7.

To discuss the tower mode shapes, a level of the tower is defined to be a plane containing four nodes with the same z-coordinate. The top of the tower is level 1 and the base of the tower is level 19. The displacement of a level could be represented by a single displacement since at the six levels having plates, the four u-displacements were specified to be equal, and at the remaining levels the u-displacements at each of the four nodes were found, from the calculations, to be equal. The latter effect was expected because the tower was designed to be symmetrical with respect to a plane normal to the x-direction and through the center line of the tower.

The tower portions of the calculated mode shapes in figures 7 to 10 were plotted by fairing curves through the displacements of the 19 levels of the tower. The experimental displacements are represented by circles. The vehicle portions of the calculated mode shapes (figs. 9 and 10) were plotted by fairing curves through the displacements of 20 stations on the vehicle. In the configurations in which the launch platform is included,

20

the displacements at the base of the tower and at the base of the vehicle represent the sway of the entire configuration of the legs of the launch platform.

Umbilical Tower Alone

The first five resonant frequencies of the umbilical tower fixed to a rigid foundation are presented in table IX. The first four corresponding mode shapes appear in figure 7. The experimental frequencies and mode shapes from reference 6 are also presented in table IX and figure 7 for comparison.

As noted in table IX, the first experimental mode did not occur solely in the plane of the tower and vehicle center lines (that is, in the x-direction). Rather, when excitation was applied in the x-direction, two first modes were observed, both of which had motion both in the x- and y-directions. Furthermore, no direction of excitation was found for which motion was confined solely to the x-direction (or for that matter to the y-direction). These two experimental modes probably represent coupled motion between the first mode in the x-direction and the first mode in the y-direction. To investigate this possibility further, the frequencies and mode shapes of the tower in the y-direction were computed. The frequencies presented for the tower in the y-direction appear in table IX along with the experimental frequencies for motion in this direction. The interesting result of this calculation is that the frequency of the first mode of the tower in the y-direction (at 26.11 Hz) and the frequency of the first mode of the tower in the x-direction (at 32.37 Hz) bracket the two experimental first-mode frequencies (at 28.2 Hz and 29.8 Hz). This result suggests that the lower coupled mode represents a raising of the frequency in the y-direction and the higher coupled mode represents a lowering of the frequency in the x-direction. The failure of the umbilical tower to have uncoupled responses in the x- and y-direction was unexpected and is thought to be due to unintentional manufacturing asymmetries.

Inspection of table IX reveals that the first modal frequency of the tower in the x-direction is calculated to be higher than the corresponding frequency in the y-direction. This difference would seem to be unexpected since the tower flares in such a way that at its lower end the dimension measured in the x-direction is smaller than the corresponding dimension in the y-direction. The stiffness in the x-direction thus might be expected to be less than the stiffness in the y-direction (by analogy with a beam), and therefore would lead to a higher first modal frequency in the y-direction. However, a static test on the tower (described in ref. 6) revealed that when the tower was loaded identically in the two directions, deflections were smaller in the x-direction than in the y-direction. Therefore, the tower is stiffer in the x-direction.

Generally, good agreement was found between the analytical and experimental results for the umbilical tower fixed to a rigid foundation. No percentage difference is

listed for the first mode in either the x- or y-directions, in accordance with previous remarks concerning these modes. In figure 7 the first experimental mode shape shown is a projection of the first experimental mode shape onto the plane of the vehicle and tower center lines.

Tower on Launch Platform

The first four resonant frequencies of the umbilical tower on the launch platform are presented in table IX and the corresponding mode shapes are presented in figure 8. The displacement of the launch platform is plotted at the base of the tower and launch platform and on the legs of the launch platform.

As noted in table IX, the first experimental mode did not occur solely in the plane of the tower and vehicle center lines. Whereas the launch platform did have motion only in the x-direction, the tower was observed to have motion in both the x- and y-directions when the system was excited in the x-direction. This motion indicates that the out-of-plane response of the umbilical-tower—launch-platform configuration is not caused by the nonsymmetrical arrangement of the legs and cylindrical weights of the launch platform but rather by the asymmetries of the umbilical tower.

Mounting the umbilical tower on the launch platform had little effect on the tower frequencies since the frequencies of the tower—launch-platform system are nearly the same as those of the tower fixed to a rigid foundation. (See table IX.) This similarity indicates that the launch platform acts essentially as a rigid foundation for the tower.

The comparison between the analytical and experimental frequencies for the tower-launch platform system is shown in table IX. No percentage difference is listed for the first mode since it did not occur in the plane of the analysis. The agreement between analysis and experiment for the remaining frequencies, which did occur in the plane of the analysis, is considered good. The comparison between the analytical and experimental mode shapes is shown in figure 8. The first experimental mode shown in figure 8 is the projection of that nonplanar mode onto the plane of the analysis. The agreement between the experimental and analytical mode shapes is also generally seen to be good.

Saturn V Vehicle Alone

The first six resonant frequencies of the model of the Saturn V vehicle are presented in table IX. The mode shapes are shown in figure 9. The shape of the mode at 13.1 Hz is not shown in figure 9 since it does not differ from the first mode except that the branches corresponding to the two fuel-slosh mechanisms in the first stage have finite deflections. This branch mode is identical to the one shown in figure 10(b). The weight conditions of the vehicle for this calculation are that the first-stage tanks are 85 percent full and the remaining tanks are 100 percent full. The boundary condition,

22

although referred to as fixed to a rigid foundation, is more specifically one in which the lower end may not translate but is able to rotate against a rotational spring. The determination of the spring constant is discussed in reference 7.

The results for the vehicle alone are included in this report primarily to demonstrate the influence of the vehicle motion on the coupled motion of the complete umbilical-tower—launch-platform—vehicle configuration. Nevertheless, a comparison of the results for the vehicle alone with experimental results of reference 7 is included in table XI and figure 9. The calculated results are in good agreement with the experimental findings.

Tower, Platform, and Vehicle

The first eight resonant frequencies of the complete umbilical-tower—launch-platform—vehicle configuration are presented in table IX. The corresponding mode shapes are shown in figure 10. The displacement of the launch platform represents the rigid-body sway of the entire configuration on the legs of the launch platform. Each mode shape is normalized to the maximum displacement. The experimental displacements from reference 6 are plotted in figure 10 as circles.

As noted in table IX, for the mode in which the tower motion is uncoupled from the motion of the launch platform and vehicle, the tower was observed experimentally to have motion out of the plane of the analysis. This motion was expected, since similar out-of-plane response was observed in both the tower alone and the tower-launch platform experiments. The remaining modes shown in figure 10 did have responses that were confined to the plane of the tower and vehicle center lines. The experimental data shown in figure 10(a) (that is, the third mode) represent the projection of the nonplanar motion onto the plane of the analysis.

The mode which occurred at the calculated frequency of 13.00 Hz (fig. 10(b)) is one in which the motion of the two fuel-slosh mechanisms is coupled with the first bending mode of the main-vehicle structure. This mode shape is identical to the mode which occurred at 13.09 Hz for the vehicle alone.

To compute the value of the rotational spring R, which connects the vehicle to the launch platform, a trial-and-error procedure was used in which a trial spring constant was inserted into equation (7), the resulting spring matrix inserted into the matrix, and the frequencies of the configuration computed. The value of the spring that gave good agreement between the computed and experimental frequencies for the first uncoupled vehicle mode, $f_e = 9.50$ Hz (fig. 10(a)), was taken to be the rotational-spring constant for the vehicle tiedown point. With this value of the spring constant used, all the remaining modes of the configuration involving the vehicle came into good agreement with the experimental results. The spring constant was determined to be 9.0×10^6 lb/in.

23

(15.8 $\times$ 10^8 N/m). To see the effect of neglecting this spring at the vehicle tiedown point, a calculation was made under the assumption of a cantilever end condition for the vehicle (that is, an infinite rotational-spring constant) and the results are presented in table IX.

Of the eight modes presented in figure 10, six represent uncoupled motion of either the vehicle or the umbilical tower. If the uncoupled modes are considered first, table IX and figures 7, 8, and 10, show that the frequency of the first tower mode is independent of whether the tower is fixed to a rigid foundation or mounted on the launch platform with or without the vehicle. Also, table IX and figures 9 and 10 show that the frequencies of the higher modes of the vehicle are essentially independent of whether the vehicle is fixed to a foundation or mounted on the launch platform with the umbilical tower. The first vehicle frequency, however, is significantly affected by placing the vehicle on the launch platform. This effect was not unexpected since the vehicle was assumed to act as a beam and the first mode of a beam is known to be very sensitive to the end conditions whereas the higher modes are affected to a lesser degree. The first coupled mode is the sixth system mode and analytically occurs at 75.43 Hz. This mode represents the coupling between the third vehicle mode shown with a frequency of 68.54 Hz (fig. 9(c)) and the second tower mode shown with a frequency of 76.59 Hz (fig. 7(b)). The other coupled mode occurs at 130.7 Hz and represents the coupling between the fourth vehicle mode shown in figure 9(d) with a frequency of 114.7 Hz and the third tower mode shown in figure 7(c) with a frequency of 133.5 Hz.

The experimental results tend to verify the analytical results for the complete configuration. The agreement is better for the uncoupled modes than for the coupled modes; this result is understandable since the first coupled mode is actually the sixth natural mode of the system, and better agreement is expected for the lower modes.

CONCLUSIONS

On the basis of the vibration analysis of a 1/40-scale model of the Saturn V—umbilical-tower—launch-platform configuration and the comparison of the results with experiment, several observations can be made.

1. The agreement between the analytical and experimental results indicates that the direct stiffness method provides an effective technique for predicting the vibration characteristics of complex structures, such as a launch vehicle and its supporting structure.

2. It was revealed by the analysis and verified by experiment that the lowest five modes of the complete configuration consist of uncoupled motion of either the vehicle or the umbilical tower.

3. The joining condition between the vehicle and the launch platform was found to be critical for the calculated values of the vehicle frequencies. The effect of this joining condition could not be defined by a simple cantilever condition but was represented by a rotational spring.

4. The attempt to verify experimentally the analytical frequency and mode shape of the first tower mode revealed that the tower did not have a first-mode response in the plane of the tower and vehicle center lines. Instead, the tower responded in two first modes which evidently represented coupling between the first mode in the plane of the tower and vehicle center lines and the first mode in the normal plane. A calculation of the frequency of the mode in the normal plane revealed that the frequencies of the modes in the two planes bracketed the experimental frequencies for the first mode. The proposed explanation for the nonplanar behavior of the tower in the first mode is that the tower contained manufacturing asymmetries which were not taken into account in the analysis.

Langley Research Center,
     National Aeronautics and Space Administration,
          Langley Station, Hampton, Va., May 21, 1968,
               124-08-05-18-23.

REFERENCES

1. Turner, M. J.; Clough, R. W.; Martin, H. C.; and Topp, L. J.: Stiffness and Deflection Analysis of Complex Structures. J. Aeron. Sci., vol. 23, no. 9, Sept. 1956, pp. 805-823.

2. Hurty, Walter C.; and Rubinstein, Moshe F.: Dynamics of Structures. Prentice-Hall, Inc., c.1964.

3. Melosh, Robert J.; and Christiansen, Henry N.: Structural Analysis and Matrix Interpretive System (SAMIS) Program: Technical Report. Tech. Mem. No. 33-311 (Contract NAS 7-100), Jet Propulsion Lab., California Inst. Technol., Nov. 1, 1966.

4. Melosh, Robert J.; Diether, Philip A.; and Brennan, Mary: Structural Analysis and Matrix Interpretive System (SAMIS) Program Report. Tech. Mem. No. 33-307, Revision 1 (Contract NAS 7-100), Jet Propulsion Lab., California Inst. Technol., Dec. 15, 1966.

5. Lang, Theodore E.: Structural Analysis and Matrix Interpretive System (SAMIS) User Report. Tech. Mem. No. 33-305 (Contract NAS 7-100), Jet Propulsion Lab., California Inst. Technol., Mar. 1, 1967.

6. Catherines, John J.: Experimental Vibration Characteristics of a 1/40-Scale Dynamic Model of the Saturn—Launch-Umbilical-Tower Configuration. NASA TN D-4870, 1968.

7. Steeves, Earl C.; and Catherines, John J.: Lateral Vibration Characteristics of a 1/40-Scale Dynamic Model of Apollo-Saturn V Launch Vehicle. NASA TN D-4872, 1968.

TABLE I.- AREAS OF ELEMENTS OF TOWER

[If W or N is not specified then property is same for both sides]

Elements
B – Brace
H – Horizontal
V – Vertical
D – Diagonal
W – Wide side
N – Narrow side
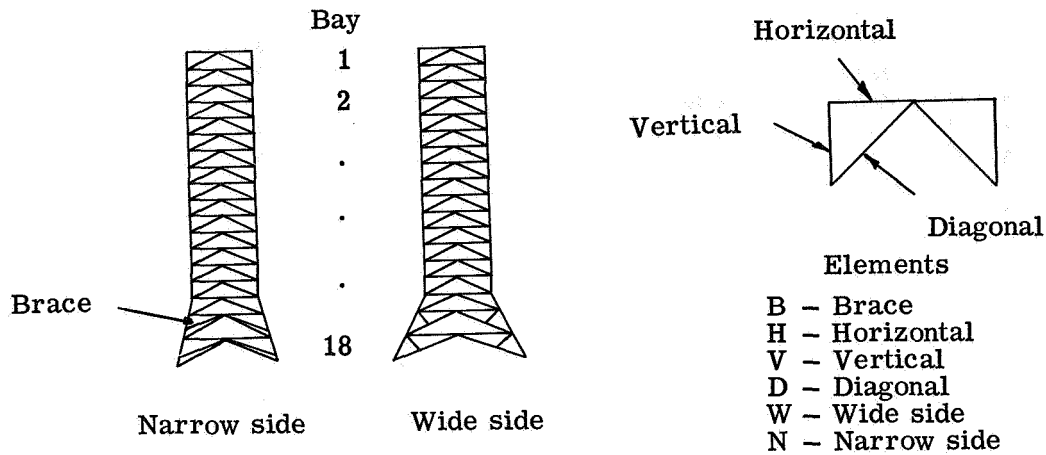
Bay and element	Area		Bay and element	Area		Bay and element	Area	
	in²	cm²		in²	cm²		in²	cm²
1H	0.0727	0.469	8H	0.056	0.361	15H	0.073	0.471
1V	.045	.290	8V	.241	1.55	15V	.69	4.45
1D	.024	.155	8D	.048	.310	15D	.065	.419
2H	.0499	.322	9H	.0617	.398	16HW	.345	2.23
2V	.045	.290	9V	.292	1.88	16VW	.815	5.26
2D	.0244	.157	9D	.048	.310	16DW	.141	.910
3H	.0499	.322	10H	.0617	.398	16HN	.095	.613
3V	.082	.529	10V	.345	2.23	16VN	.815	5.26
3D	.0244	.157	10D	.048	.310	16DN	.046	.297
4H	.0499	.322	11H	.069	.445	17HW	.110	.710
4V	.082	.529	11V	.400	2.58	17VW	.815	5.26
4D	.0244	.157	11D	.048	.310	17DW	.100	.645
5H	.0499	.322	12H	.069	.445	17HN	.056	.361
5V	.142	.916	12V	.436	2.81	17VN	.815	5.26
5D	.032	.206	12D	.048	.310	17DN	.046	.297
6H	.0499	.322	13H	.069	.445	18HW	.110	.710
6V	.142	.916	13V	.512	3.30	18VW	.815	5.26
6D	.032	.206	13D	.065	.419	18DW	.039	.252
7H	.056	.361	14H	.073	.471	18HN	.056	.361
7V	.19	1.23	14V	.571	3.68	18VN	.815	5.26
7D	.032	.206	14D	.065	.419	18DN	.458	2.95
						17B	.014	.0903
						18B	.014	.0903

TABLE II.- NODAL COORDINATES OF UMBILICAL TOWER

Node	x		y		z	
	in.	cm	in.	cm	in.	cm
1	0	0	0	0	90.0	228.6
2	12.0	30.48	0	0	90.0	228.6
3	12.0	30.48	12.0	30.48	90.0	228.6
4	0	0	12.0	30.48	90.0	228.6
5	6.0	15.24	0	0	90.0	228.6
6	12.0	30.48	6.0	15.24	90.0	228.6
7	6.0	15.24	12.0	30.48	90.0	228.6
8	0	0	6.0	15.24	90.0	228.6
9	0	0	0	0	84.0	213.36
10	12.0	30.48	0	0	84.0	213.36
11	12.0	30.48	12.0	30.48	84.0	213.36
12	0	0	12.0	30.48	84.0	214.36
13	6.0	15.24	0	0	84.0	213.36
14	12.0	30.48	6.0	15.24	84.8	213.36
15	6.0	15.24	12.0	30.48	84.0	213.36
16	0	0	6.0	15.24	84.0	213.36
17	0	0	0	0	78.0	198.12
18	12.0	30.48	0	0	78.0	198.12
19	12.0	30.48	12.0	30.48	78.0	198.12
20	0	0	12.0	30.48	78.0	198.12
21	6.0	15.24	0	0	78.0	198.12
22	12.0	30.48	6.0	15.24	78.0	198.12
23	6.0	15.24	12.0	30.48	78.0	198.12
24	0	0	6.0	15.24	78.0	198.12
25	0	0	0	0	72.0	182.88
26	12.0	30.48	0	0	72.0	182.88
27	12.0	30.48	12.0	30.48	72.0	182.88
28	0	0	12.0	30.48	72.0	182.88
29	6.0	15.24	0	0	72.0	182.88
30	12.0	30.48	6.0	15.24	72.0	182.88
31	6.0	15.24	12.0	30.48	72.0	182.88
32	0	0	6.0	15.24	72.0	182.88
33	0	0	0	0	66.0	167.64
34	12.0	30.48	0	0	66.0	167.64
35	12.0	30.48	12.0	30.48	66.0	167.64
36	0	0	12.0	30.48	66.0	167.64
37	6.0	15.24	0	0	66.0	167.64
38	12.0	30.48	6.0	15.24	66.0	167.64
39	6.0	15.24	12.0	30.48	66.0	167.64
40	0	0	6.0	15.24	66.0	167.64
41	0	0	0	0	60.0	152.40
42	12.0	30.48	0	0	60.0	152.40
43	12.0	30.48	12.0	30.48	60.0	152.40
44	0	0	12.0	30.48	60.0	152.40
45	6.0	15.24	0	0	60.0	152.40
46	12.0	30.48	6.0	15.24	60.0	152.40
47	6.0	15.24	12.0	30.48	60.0	152.40
48	0	0	6.0	15.24	60.0	152.40
49	0	0	0	0	54.0	137.16
50	12.0	30.48	0	0	54.0	137.16

TABLE II.- NODAL COORDINATES OF UMBILICAL TOWER — Continued

Node	x		y		z	
	in.	cm	in.	cm	in.	cm
51	12.0	30.48	12.0	30.48	54.0	137.16
52	0	0	12.0	30.48	54.0	137.16
53	6.0	15.24	0	0	54.0	137.16
54	12.0	30.48	6.0	15.24	54.0	137.16
55	6.0	15.24	12.0	30.48	54.0	137.16
56	0	0	6.0	15.24	54.0	137.16
57	0	0	0	0	48.0	121.92
58	12.0	30.48	0	0	48.0	121.92
59	12.0	30.48	12.0	30.48	48.0	121.92
60	0	0	12.0	30.48	48.0	121.92
61	6.0	15.24	0	0	48.0	121.92
62	12.0	30.48	6.0	15.24	48.0	121.92
63	6.0	15.24	12.0	30.48	48.0	121.92
64	0	0	6.0	15.24	48.0	121.92
65	0	0	0	0	42.0	106.68
66	12.0	30.48	0	0	42.0	106.68
67	12.0	30.48	12.0	30.48	42.0	106.68
68	0	0	12.0	30.48	42.0	106.68
69	6.0	15.24	0	0	42.0	106.68
70	12.0	30.48	6.0	15.24	42.0	106.68
71	6.0	15.24	12.0	30.48	42.0	106.68
72	0	0	6.0	15.24	42.0	106.68
73	0	0	0	0	36.0	91.44
74	12.0	30.48	0	0	36.0	91.44
75	12.0	30.48	12.0	30.48	36.0	91.44
76	0	0	12.0	30.48	36.0	91.44
77	6.0	15.24	0	0	36.0	91.44
78	12.0	30.48	6.0	15.24	36.0	91.44
79	6.0	15.24	12.0	30.48	36.0	91.44
80	0	0	6.0	15.24	36.0	91.44
81	0	0	0	0	30.0	76.20
82	12.0	30.48	0	0	30.0	76.20
83	12.0	30.48	12.0	30.48	30.0	76.20
84	0	0	12.0	30.48	30.0	76.20
85	6.0	15.24	0	0	30.0	76.20
86	12.0	30.48	6.0	15.24	30.0	76.20
87	6.0	15.24	12.0	30.48	30.0	76.20
88	0	0	6.0	15.24	30.0	76.20
89	0	0	0	0	24.0	60.96
90	12.0	30.48	0	0	24.0	60.96
91	12.0	30.48	12.0	30.48	24.0	60.96
92	0	0	12.0	30.48	24.0	60.96
93	6.0	15.24	0	0	24.0	60.96
94	12.0	30.48	6.0	15.24	24.0	60.96
95	6.0	15.24	12.0	30.48	24.0	60.96
96	0	0	6.0	15.24	24.0	60.96
97	0	0	0	0	18.0	45.72
98	12.0	30.48	0	0	18.0	45.72
99	12.0	30.48	12.0	30.48	18.0	45.72
100	0	0	12.0	30.48	18.0	45.72

TABLE II.- NODAL COORDINATES OF UMBILICAL TOWER -- Concluded

Node	x		y		z	
	in.	cm	in.	cm	in.	cm
101	6.0	15.24	0	0	18.0	45.72
102	12.0	30.48	6.0	15.24	18.0	45.72
103	6.0	15.24	12.0	30.48	18.0	45.72
104	0	0	6.0	15.24	18.0	45.72
105	0	0	0	0	12.0	30.48
106	12.0	30.48	0	0	12.0	30.48
107	12.0	30.48	12.0	30.48	12.0	30.48
108	0	0	12.0	30.48	12.0	30.48
109	6.0	15.24	0	0	12.0	30.48
110	12.0	30.48	6.0	15.24	12.0	30.48
111	6.0	15.24	12.0	30.48	12.0	30.48
112	0	0	6.0	15.24	12.0	30.48
113	0	0	0	0	6.0	15.24
114	12.0	30.48	0	0	6.0	15.24
115	12.0	30.48	12.0	30.48	6.0	15.24
116	0	0	12.0	30.48	6.0	15.24
117	6.0	15.24	0	0	6.0	15.24
118	12.0	30.48	6.0	15.24	6.0	15.24
119	6.0	15.24	12.0	30.48	6.0	15.24
120	0	0	6.0	15.24	6.0	15.24
121	0	0	0	0	0	0
122	12.0	30.48	0	0	0	0
123	12.0	30.48	12.0	30.48	0	0
124	0	0	12.0	30.48	0	0
125	0	0	6.0	15.24	0	0
126	6.0	15.24	0	0	0	0
127	12.0	30.48	6.0	15.24	0	0
128	6.0	15.24	12.0	30.48	0	0
129	-.812	-2.06	14.687	37.30	-5.304	-13.47
130	-.812	-2.06	6.0	15.24	-5.304	-13.47
131	-.812	-2.06	-2.687	-6.825	-5.304	-13.47
132	6.0	15.24	-2.687	-6.825	-5.304	-13.47
133	12.812	32.54	-2.687	-6.825	-5.304	-13.47
134	12.812	32.54	6.0	15.24	-5.304	-13.47
135	12.812	32.54	14.687	37.30	-5.304	-13.47
136	6.0	15.24	14.687	37.30	-5.304	-13.47
137	.562	1.43	12.406	31.51	-9.088	-23.08
138	.562	1.43	-.406	-1.03	-9.088	-23.08
139	13.374	33.97	-.406	-1.03	-9.088	-23.08
140	13.374	33.97	12.406	31.51	-9.088	-23.08
141	-1.937	-4.920	18.812	47.782	-12.873	-32.697
142	-12.873	-32.697	6.0	15.24	-12.873	-32.697
143	-1.937	-4.920	-6.812	-17.302	-12.873	-32.697
144	6.0	15.24	-6.812	-17.302	-12.873	-32.697
145	13.937	35.400	-6.812	-17.302	-12.873	-32.697
146	13.937	35.400	6.0	15.24	-12.873	-32.697
147	13.937	35.400	18.812	47.782	-12.873	-32.697
148	6.0	15.24	18.812	47.782	-12.873	-32.697
149	-2.468	-6.269	14.812	37.622	-17.072	-43.363
150	-2.468	-6.269	-2.812	-7.142	-17.072	-43.363
151	14.468	36.749	-2.812	-7.142	-17.072	-43.363
152	14.468	36.749	14.812	37.622	-17.072	-43.363
153	-3.0	-7.62	23.625	60.007	-21.271	-54.028
154	-3.0	-7.62	-11.625	-29.528	-21.271	-54.028
155	15.0	38.10	-11.625	-29.528	-21.271	-54.028
156	15.0	38.10	23.625	60.007	-21.271	-54.028

30

TABLE III.- LAUNCH-PLATFORM-SECTION PROPERTIES

Local coordinate system for element
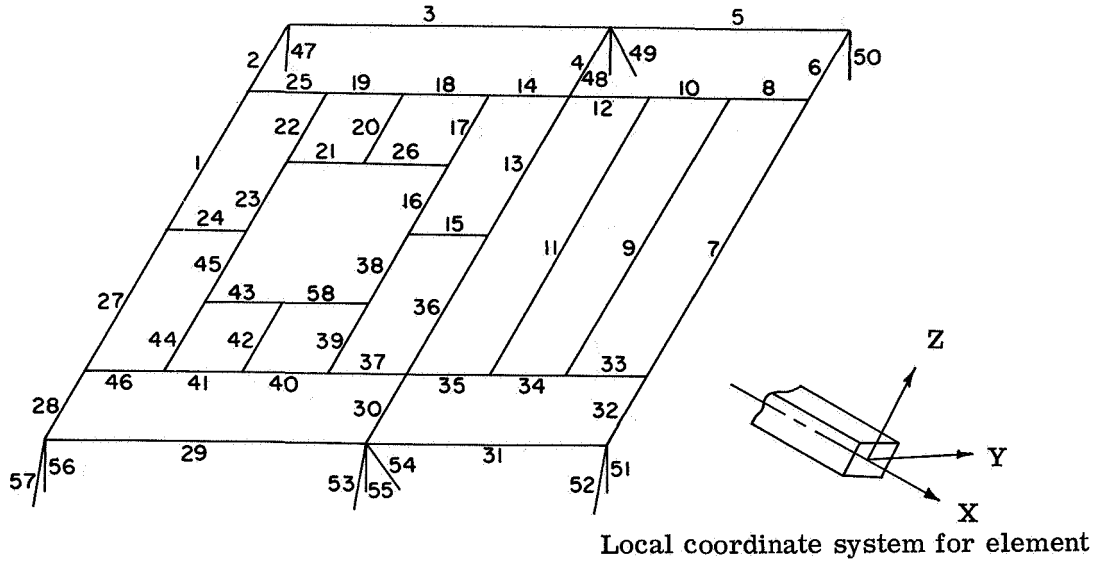
Element no.	A_X		I_Y		I_Z	
	in^2	cm^2	in^4	cm^4	in^4	cm^4
1	1.508	9.729	11.19	465.763	0.045	1.873
2	1.508	9.729	11.19	465.763	.045	1.873
3	.720	4.65	3.08	128.199	.022	.916
4	1.373	8.858	10.04	417.896	.082	3.413
5	.720	4.65	3.08	128.199	.022	.916
6	1.05	6.774	7.28	303.02	.047	1.956
7	1.05	6.774	7.28	303.02	.047	1.956
8	1.05	6.774	7.28	303.02	.047	1.956
9	.062	.400	1.76	73.257	.003	.125
10	1.05	6.774	7.28	303.02	.047	1.956
11	.062	.400	1.76	73.257	.003	.125
12	1.05	6.774	7.28	303.02	.047	1.956
13	1.373	8.858	10.04	417.896	.082	3.413
14	.947	6.11	7.67	319.250	.101	4.204
15	1.200	7.74	6.36	264.723	.041	1.707
16	1.808	11.664	6.44	268.053	.114	4.745
17	1.808	11.664	6.44	268.053	.114	4.745
18	.830	5.353	6.00	249.739	.143	5.952
19	1.068	6.889	5.51	229.344	.129	5.37
20	1.2	7.74	6.36	264.723	.041	1.707

TABLE III.- LAUNCH-PLATFORM-SECTION PROPERTIES – Concluded

Element no.	A_X		I_Y		I_Z	
	in^2	cm^2	in^4	cm^4	in^4	cm^4
21	0.975	6.290	6.58	273.880	0.057	2.373
22	.890	5.303	6.44	268.053	.117	4.870
23	.890	5.303	6.44	268.053	.117	4.870
24	1.222	7.882	8.98	373.568	.065	2.704
25	1.296	8.359	10.43	433.888	.122	5.075
26	.975	6.289	6.58	273.880	.057	2.371
27	1.508	9.729	11.19	465.663	.045	1.873
28	1.508	9.729	11.19	465.663	.045	1.873
29	.720	4.65	3.08	128.199	.022	.916
30	1.373	8.858	10.04	417.896	.082	3.413
31	.720	4.65	3.08	128.199	.022	.916
32	1.05	6.774	7.28	303.02	.047	1.956
33	1.05	6.774	7.28	303.02	.047	1.956
34	1.05	6.774	7.28	303.02	.047	1.956
35	1.05	6.774	7.28	303.02	.047	1.956
36	1.373	8.858	10.04	417.896	.082	3.413
37	.947	6.108	7.67	319.250	.101	4.204
38	1.808	11.664	6.44	268.053	.114	4.745
39	1.808	11.664	6.44	268.053	.114	4.745
40	.83	5.354	6.00	249.739	.143	5.952
41	1.068	6.889	5.51	229.344	.129	5.37
42	1.2	7.74	6.36	264.723	.049	2.038
43	.975	6.289	6.58	273.880	.057	2.371
44	.890	5.303	6.44	268.053	.117	4.870
45	.890	5.303	6.44	268.053	.117	4.870
46	1.296	8.359	10.43	433.888	.122	5.075
47	.994	6.441	.078	3.244	.078	3.244
48	.994	6.441	.078	3.244	.078	3.244
49	.307	1.980	.007	.291	.007	.291
50	.994	6.441	.078	3.244	.078	3.244
51	.994	6.441	.078	3.244	.078	3.244
52	.307	1.980	.007	.291	.007	.291
53	.307	1.980	.007	.291	.007	.291
54	.307	1.980	.007	.291	.007	.291
55	.994	6.441	.078	3.244	.078	3.244
56	.994	6.441	.078	3.244	.078	3.244
57	.307	1.980	.007	.291	.007	.291
58	.975	6.289	6.58	273.890	.057	2.373

TABLE IV.- NODAL COORDINATES OF LAUNCH PLATFORM

Node	X		Y		Z	
	in.	cm	in.	cm	in.	cm
1	40.2	102	-7.2	-18.3	0	0
2	40.2	102	0	0	0	0
3	33.0	83.8	-7.2	-18.3	0	0
4	33.0	83.8	7.2	18.3	0	0
5	40.2	102	-13.4	-34.0	0	0
6	47.4	120	0	0	0	0
7	40.2	102	7.2	18.3	0	0
8	47.4	120	13.4	34.0	0	0
9	25.8	65.5	7.2	18.3	0	0
10	33.0	83.8	-13.4	-34.0	0	0
11	25.8	65.5	-7.2	-18.3	0	0
12	33.4	83.8	13.4	34.0	0	0
13	40.2	102	13.4	34.0	0	0
14	47.4	120	-13.4	-34.0	0	0
15	25.8	65.5	0	0	0	0
16	47.4	120	19.95	50.7	0	0
17	25.8	65.5	13.4	34.0	0	0
18	25.8	65.5	-13.4	-34.0	0	0
19	47.4	120	19.95	50.7	8.375	21.27
20	47.4	120	-25.2	-64.0	8.375	21.27
21	18	45.7	0	0	0	0
22	47.4	120	-19.95	-50.7	0	0
23	47.4	120	-19.95	-50.7	8.375	21.27
24	18	45.7	19.95	50.7	0	0
25	18	45.7	13.4	34.0	0	0
26	18	45.7	-13.4	-34.0	0	0
27	18	45.7	19.95	50.7	8.375	21.27
28	12	30.5	-13.4	-34.0	0	0
29	9.13	23.2	19.95	50.7	8.375	21.27
30	18	45.7	-19.95	-50.7	0	0
31	12	30.5	13.4	34.0	0	0
32	0	0	19.95	50.7	0	0
33	6	15.24	13.4	34.0	0	0
34	18	45.7	-25.2	-64.0	8.375	21.27
35	9.13	23.2	-19.95	-50.7	8.375	21.27
36	6	15.24	-13.4	-34.0	0	0
37	0	0	-19.95	-50.7	0	0
38	0	0	13.4	34.0	0	0
39	0	0	-13.4	-34.0	0	0
40	0	0	-19.95	-50.7	8.375	21.27
41	0	0	-25.2	-64.0	8.375	21.27
42	18	45.7	-19.95	-50.7	8.375	21.27
43	0	0	19.95	50.7	8.375	21.27

TABLE V.- REDUCED STIFFNESS MATRIX FOR 1/40-SCALE SATURN V LAUNCH VEHICLE

[Each number is followed by the letter E (for exponent), a minus symbol or a blank space (for plus), and two digits that indicate the power of 10 by which the number must be multiplied to obtain the correct value]

(a) U.S. Customary Units

ROW	1	2	3	4	5	6	7	8
1	0.70942000E 03	0.00000000E-38	0.00000000E-38	0.00000000E-38	0.00000000E-38	0.00000000E-38	0.00000000E-38	0.00000000E-38
2	0.00000000E-38	0.44247000E 04	0.00000000E-38	0.00000000E-38	0.00000000E-38	0.00000000E-38	0.00000000E-38	0.00000000E-38
3	0.00000000E-38	0.00000000E-38	0.31000000E 03	0.00000000E-38	0.00000000E-38	0.00000000E-38	0.00000000E-38	0.00000000E-38
4	0.00000000E-38	0.00000000E-38	0.00000000E-38	0.31000000E 03	0.00000000E-38	0.00000000E-38	0.00000000E-38	0.00000000E-38
5	0.00000000E-38	0.00000000E-38	0.00000000E-38	0.00000000E-38	0.21870000E 05	0.00000000E-38	0.00000000E-38	0.00000000E-38
6	0.00000000E-38	0.00000000E-38	0.00000000E-38	0.00000000E-38	0.00000000E-38	0.57951260E 04	-0.11279710E 05	0.66599013E 04
7	0.00000000E-38	0.00000000E-38	0.00000000E-38	0.00000000E-38	0.00000000E-38	-0.11279710E 05	0.28894677E 05	-0.27067598E 05
8	0.00000000E-38	0.00000000E-38	0.00000000E-38	0.00000000E-38	0.00000000E-38	0.66599013E 04	-0.27067598E 05	0.45205623E 05
9	0.00000000E-38	0.00000000E-38	0.00000000E-38	0.00000000E-38	0.00000000E-38	-0.12135442E 04	-0.97600726E 04	-0.34483819E 05
10	0.00000000E-38	0.00000000E-38	0.00000000E-38	0.00000000E-38	0.00000000E-38	0.39454887E 02	-0.31732060E 03	0.99971165E 04
11	0.00000000E-38	0.00000000E-38	0.00000000E-38	0.00000000E-38	0.00000000E-38	-0.12517756E 01	0.10067554E 02	-0.31717609E 03
12	0.00000000E-38	0.00000000E-38	0.00000000E-38	0.00000000E-38	0.00000000E-38	0.15637542E-01	-0.12576678E 00	0.39622553E 01
13	0.00000000E-38	0.00000000E-38	0.00000000E-38	0.00000000E-38	0.00000000E-38	0.21003265E-02	-0.16892124E-01	0.53218270E 00
14	0.00000000E-38	0.00000000E-38	0.00000000E-38	0.00000000E-38	0.00000000E-38	0.33722900E-02	-0.27122041E-01	0.85447402E 00
15	0.00000000E-38	0.00000000E-38	0.00000000E-38	0.00000000E-38	0.00000000E-38	0.17014888E-02	-0.13684425E-01	0.43112484E 00
16	0.00000000E-38	0.00000000E-38	0.00000000E-38	0.00000000E-38	0.00000000E-38	0.55759965E-03	-0.44845612E-02	0.14128515E 00
17	-0.70942000E 03	0.00000000E-38	0.00000000E-38	0.00000000E-38	0.00000000E-38	0.11246945E-03	-0.90454883E-03	0.28497615E-01
18	0.00000000E-38	0.00000000E-38	0.00000000E-38	0.00000000E-38	0.00000000E-38	0.80611104E-05	-0.64832433E-04	0.20425318E-02
19	0.00000000E-38	-0.44247000E 04	0.00000000E-38	0.00000000E-38	0.00000000E-38	0.27218368E-05	-0.21890694E-04	0.68966158E-03
20	0.00000000E-38	0.00000000E-38	0.00000000E-38	0.00000000E-38	0.00000000E-38	0.10470482E-05	-0.84210088E-05	0.26530206E-03
21	0.00000000E-38	0.00000000E-38	-0.31000000E 03	0.00000000E-38	0.00000000E-38	0.30047332E-06	-0.24165922E-05	0.76134212E-04
22	0.00000000E-38	0.00000000E-38	0.00000000E-38	0.00000000E-38	0.00000000E-38	0.77944738E-07	-0.62687977E-06	0.19749711E-04
23	0.00000000E-38	0.00000000E-38	0.00000000E-38	-0.31000000E 03	0.00000000E-38	0.18668875E-07	-0.15014663E-06	0.47303369E-05
24	0.00000000E-38	0.00000000E-38	0.00000000E-38	0.00000000E-38	0.00000000E-38	0.56034519E-08	-0.45066423E-07	0.14198078E-05
25	0.00000000E-38	0.00000000E-38	0.00000000E-38	0.00000000E-38	-0.21870000E 05	0.31532758E-08	-0.25360594E-07	0.79998002E-06
26	0.00000000E-38	0.00000000E-38	0.00000000E-38	0.00000000E-38	0.00000000E-38	0.46440380E-07	-0.37350225E-06	0.11767107E-04

TABLE V.- REDUCED STIFFNESS MATRIX FOR 1/40-SCALE SATURN V LAUNCH VEHICLE – Continued

(a) U.S. Customary Units – Continued

ROW	COL 9	10	11	12	13	14	15	16
1	0.00000000E-38	0.00000000E-38	0.00000000E-38	0.00000000E-38	0.00000000E-38	0.00000000E-38	0.00000000E-38	0.00000000E-38
2	0.00000000E-38	0.00000000E-38	0.00000000E-38	0.00000000E-38	0.00000000E-38	0.00000000E-38	0.00000000E-38	0.00000000E-38
3	0.00000000E-38	0.00000000E-38	0.00000000E-38	0.00000000E-38	0.00000000E-38	0.00000000E-38	0.00000000E-38	0.00000000E-38
4	0.00000000E-38	0.00000000E-38	0.00000000E-38	0.00000000E-38	0.00000000E-38	0.00000000E-38	0.00000000E-38	0.00000000E-38
5	0.00000000E-38	0.00000000E-38	0.00000000E-38	0.00000000E-38	0.00000000E-38	0.00000000E-38	0.00000000E-38	0.00000000E-38
6	-0.12135442E 04	0.39454887E 02	-0.12517756E 01	0.15637542E-01	0.21003265E-02	0.33722900E-02	0.17014888E-02	0.55759965E-03
7	0.97600726E 04	-0.31732060E 03	0.10067554E 02	-0.12576678E 00	-0.16892124E-01	-0.27122041E-01	-0.13684425E-01	-0.44845612E-02
8	0.34483819E 05	0.99971165E 04	-0.31717609E 03	0.39622553E 01	0.53218270E 00	0.85447402E 00	0.43112484E 00	0.14128513E 00
9	0.51866257E 05	-0.38833461E 05	0.80556886E 04	-0.10063399E 03	-0.13516461E 02	-0.21702066E 02	-0.10949777E 02	-0.35883821E 01
10	-0.33833461E 05	0.48846095E 05	-0.30254297E 05	0.36757106E 04	0.49369601E 03	0.79267966E 03	0.39994650E 03	0.13106759E 03
11	0.80556886E 04	-0.30254297E 05	0.47341492E 05	-0.28786467E 05	-0.10565098E 04	0.16963350E 04	0.85588578E 03	0.28048473E 03
12	-0.10063399E 03	0.36757106E 04	-0.28786467E 05	0.36531110E 05	-0.33076268E 05	0.22093539E 04	0.11147294E 04	0.36531110E 03
13	-0.13516461E 02	0.49369601E 03	-0.10565098E 04	-0.33076268E 05	0.73712356E 05	-0.47352051E 05	0.36964589E 04	0.12113769E 04
14	-0.21702066E 02	0.79267966E 03	0.16963350E 04	0.22093539E 04	-0.47352051E 05	0.83254880E 05	-0.41733366E 05	-0.94229842E 04
15	-0.10949777E 02	0.39994650E 03	0.85588578E 03	0.11147294E 04	0.36964589E 04	-0.41733366E 05	0.46727906E 05	-0.14335014E 05
16	-0.35883821E 01	0.13106759E 03	0.28048473E 03	0.36531110E 03	0.12113769E 04	-0.94229842E 04	-0.31225062E 05	-0.29678068E 05
17	-0.72378693E 00	0.26436708E 02	0.56574572E 02	0.73684295E 02	0.24433819E 03	0.19006429E 03	0.29617687E 04	0.64965067E 04
18	-0.51876545E-01	0.18948188E 01	0.40549134E 01	0.52812319E 01	0.17512641E 02	0.13622626E 02	0.21228115E 03	0.21935478E 04
19	-0.17516134E-01	0.63978623E 00	0.13691429E 01	0.17832098E 01	0.59131495E 01	0.45996845E 01	0.71676806E 02	0.84382365E 03
20	-0.67381828E-02	0.24611579E 00	0.52668795E 00	0.68597304E 00	0.22746965E 01	0.17694269E 01	0.27572951E 02	0.24215360E 03
21	-0.19336688E-02	0.70628292E-01	0.15114460E 00	0.19685492E 00	0.65277376E 00	0.50777565E 00	0.79126592E 01	0.62816226E 02
22	-0.50160630E-03	0.18321440E-01	0.39207895E-01	0.51065452E-01	0.16933377E 00	0.13172032E 00	0.20525955E 01	0.15045380E 02
23	-0.12014185E-03	0.43882456E-02	0.93908493E-02	0.12230903E-01	0.40557849E-01	0.31548889E-01	0.49162586E 00	0.45158620E 01
24	-0.36060506E-04	0.13171293E-02	0.28186579E-02	0.36710982E-02	0.12173415E-01	0.94693804E-02	0.14756121E 00	0.25412477E 01
25	-0.20292621E-04	0.74119891E-03	0.15861662E-02	0.20658669E-02	0.68504444E-02	0.53287817E-02	0.83038318E-01	0.25412477E 01
26	-0.29886285E-03	0.10916127E-01	0.23360519E-01	0.30425388E-01	0.10089103E 00	0.78480492E-01	0.12229602E 01	0.37426634E 02

TABLE V.- REDUCED STIFFNESS MATRIX FOR 1/40-SCALE SATURN V LAUNCH VEHICLE – Continued

(a) U.S. Customary Units – Continued

ROW	COL 17	18	19	20	21	22	23	24
1	-0.70942000E 03	0.00000000E-38	0.00000000E-38	0.00000000E-38	0.00000000E-38	0.00000000E-38	0.00000000E-38	0.00000000E-38
2	0.00000000E-38	0.00000000E-38	0.00000000E-38	-0.44247000E 04	0.00000000E-38	0.00000000E-38	0.00000000E-38	0.00000000E-38
3	0.00000000E-38	0.00000000E-38	0.00000000E-38	0.00000000E 03	-0.31000000E 03	0.00000000E-38	-0.31000000E 03	0.00000000E-38
4	0.00000000E-38	0.00000000E-38	0.00000000E-38	0.00000000E-38	0.00000000E-38	0.00000000E-38	0.00000000E 03	0.00000000E-38
5	0.00000000E-38	0.00000000E-38	0.00000000E-38	0.00000000E-38	0.00000000E-38	0.00000000E-38	0.00000000E-38	0.00000000E-38
6	0.11246945E-03	0.80611104E-05	0.27218368E-05	0.10470482E-05	0.30047332E-06	0.77944738E-07	0.18668875E-07	0.56034519E-08
7	-0.90454883E-03	-0.64832433E-04	-0.21890694E-04	-0.84210088E-05	-0.24165922E-05	-0.62687977E-06	-0.15014663E-06	-0.45066423E-07
8	0.28497615E-01	0.20425318E-02	0.68966158E-03	0.26530206E-03	0.76134212E-04	0.19749711E-04	0.47303369E-05	0.14198078E-05
9	-0.72378693E 00	-0.51876545E-01	-0.17516134E-01	-0.67381838E-02	-0.19336688E-02	-0.50160630E-03	-0.12014185E-03	-0.36060506E-04
10	0.26436708E 02	0.18948188E 01	0.63978623E 00	0.24611579E 00	0.70628292E-01	0.18321440E-01	0.43882456E-02	0.13171293E-02
11	0.56574572E 02	0.40549134E 01	0.13691429E 01	0.52668795E 00	0.15114460E 00	0.39207895E-01	0.93908493E-02	0.28186579E-02
12	0.73684295E 02	0.52812319E 01	0.17832098E 01	0.68597304E 00	0.19685492E 00	0.51065452E-01	0.12230903E-01	0.36710982E-02
13	0.24433819E 03	0.17512641E 02	0.59131495E 01	0.22746965E 01	0.65277376E 00	0.16933377E 00	0.40557849E-01	0.12173415E-01
14	0.19006429E 03	0.13622626E 02	0.45996845E 01	0.17694269E 01	0.50777565E 00	0.13172032E 00	0.31548889E-01	0.94693804E-02
15	0.29617687E 04	0.21228115E 03	0.71676806E 02	0.27572951E 02	0.79126592E 01	0.20525955E 01	0.49162586E 00	0.14756121E 00
16	-0.29678068E 05	0.64965067E 04	0.21935478E 04	0.84382365E 03	0.24215360E 03	0.62816226E 02	0.15045380E 02	0.45158620E 01
17	0.78406633E 05	-0.65098686E 05	0.88195798E 04	0.33927550E 04	0.97362503E 03	0.25256470E 03	-0.60492840E 02	0.18156890E 02
18	-0.65098686E 05	0.14259857E 06	-0.10440454E 06	0.14523987E 05	0.41679748E 04	0.10811999E 04	0.25896277E 03	0.77727521E 02
19	0.88195798E 04	-0.10440454E 06	0.18344581E 06	-0.11067101E 06	0.15200283E 05	0.39430529E 04	0.94441736E 03	0.28346631E 03
20	0.33927550E 04	0.14523987E 05	-0.11067101E 06	0.20297134E 06	-0.13581474E 06	0.25656105E 05	0.21559610E 05	0.15499217E 04
21	0.97362503E 03	0.41679748E 04	0.15200283E 05	-0.13581474E 06	0.16940480E 06	0.19315176E 05	0.51638337E 04	0.57974385E 04
22	0.25256470E 03	0.10811999E 04	0.39430529E 04	0.25656105E 05	0.19315176E 05	0.28359409E 06	-0.16774827E 06	0.17058115E 05
23	-0.60492840E 02	0.25896277E 03	0.94441736E 03	0.21559610E 05	0.51638337E 04	-0.16774827E 06	0.48255137E 06	-0.36325289E 06
24	0.18156890E 02	0.77727521E 02	0.28346631E 03	0.15499217E 04	0.57974385E 04	0.17058115E 05	-0.36325289E 06	0.63580842E 06
25	0.10217574E 02	0.43740240E 02	0.15951729E 03	0.87219994E 03	0.32624394E 04	0.95992506E 04	0.23001625E 05	-0.29734491E 06
26	0.15048097E 03	0.64419141E 03	0.23493166E 04	0.12845465E 05	0.48048102E 05	0.14137451E 06	0.33876013E 06	0.11868207E 07

TABLE V.- REDUCED STIFFNESS MATRIX FOR 1/40-SCALE SATURN V LAUNCH VEHICLE -- Continued

(a) U.S. Customary Units -- Concluded

ROW	COL 25	26
1	0.00000000E-38	0.00000000E-38
2	0.00000000E-38	0.00000000E-38
3	0.00000000E-38	0.00000000E-38
4	0.00000000E-38	0.00000000E-38
5	-0.21870000E 05	0.00000000E-38
6	0.31532758E-08	0.46440380E-07
7	-0.25360594E-07	-0.37350225E-06
8	0.79898002E-06	0.11767107E-04
9	-0.20292621E-04	-0.29886285E-03
10	0.74119891E-03	0.10916127E-01
11	0.15861662E-02	0.23360519E-01
12	0.20658669E-02	0.30425388E-01
13	0.68504444E-02	0.10089103E 00
14	0.53287817E-02	0.78480492E-01
15	0.83038318E-01	0.12229602E 01
16	0.25412477E 01	0.37426634E 02
17	0.10217574E 02	0.15048097E 03
18	0.43740240E 02	0.64419141E 03
19	0.15951729E 03	0.23493166E 04
20	0.87219994E 03	0.12845465E 05
21	0.32624394E 04	0.48048102E 05
22	0.95992506E 04	0.14137451E 06
23	0.23001625E 05	0.33876013E 06
24	-0.29734491E 06	0.11868207E 07
25	0.28226333E 06	-0.17310319E 07
26	-0.17310319E 07	0.19034543E 08

TABLE V.- REDUCED STIFFNESS MATRIX FOR 1/40-SCALE SATURN V LAUNCH VEHICLE - Continued

[Each number is followed by the letter E (for exponent), a minus symbol or a blank space (for plus), and two digits that indicate the power of 10 by which the number must be multiplied to obtain the correct value]

(b) SI Units

ROW	COL 1	2	3	4	5	6	7	8
1	0.12423848E 06	0.00000000E-38	0.00000000E-38	0.00000000E-38	0.00000000E-38	0.00000000E-38	0.00000000E-38	0.00000000E-38
2	0.00000000E-38	0.77488372E 06	0.00000000E-38	0.00000000E-38	0.00000000E-38	0.00000000E-38	0.00000000E-38	0.00000000E-38
3	0.00000000E-38	0.00000000E-38	0.54289320E 05	0.54289320E 05	0.00000000E-38	0.00000000E-38	0.00000000E-38	0.00000000E-38
4	0.00000000E-38	0.00000000E-38	0.00000000E-38	0.00000000E-38	0.38300240E 07	0.00000000E-38	0.00000000E-38	0.00000000E-38
5	0.00000000E-38	0.00000000E-38	0.00000000E-38	0.00000000E-38	0.00000000E-38	0.10148821E 07	0.19753799E 07	0.11663275E 07
6	0.00000000E-38	0.00000000E-38	0.00000000E-38	0.00000000E-38	0.00000000E-38	-0.19753799E 07	0.50602335E 07	-0.47402629E 07
7	0.00000000E-38	0.00000000E-38	0.00000000E-38	0.00000000E-38	0.00000000E-38	0.11663275E 07	-0.47402629E 07	0.79167179E 07
8	0.00000000E-38	0.00000000E-38	0.00000000E-38	0.00000000E-38	0.00000000E-38	-0.21252416E 06	0.17092507E 07	-0.60390422E 07
9	0.00000000E-38	0.00000000E-38	0.00000000E-38	0.00000000E-38	0.00000000E-38	0.69096097E 04	0.55711354E 05	0.17507634E 07
10	0.00000000E-38	0.00000000E-38	0.00000000E-38	0.00000000E-38	0.00000000E-38	-0.21921951E 03	0.17630988E 04	-0.55546046E 05
11	0.00000000E-38	0.00000000E-38	0.00000000E-38	0.00000000E-38	0.00000000E-38	0.27385534E 01	-0.22025139E 02	0.69389724E 03
12	0.00000000E-38	0.00000000E-38	0.00000000E-38	0.00000000E-38	0.00000000E-38	0.36782354E 00	0.29582643E 01	0.93199474E 02
13	0.00000000E-38	0.00000000E-38	0.00000000E-38	0.00000000E-38	0.00000000E-38	0.59057848E 00	-0.47497973E 01	0.14964133E 03
14	0.00000000E-38	0.00000000E-38	0.00000000E-38	0.00000000E-38	0.00000000E-38	0.29797636E 00	-0.23965101E 01	0.75501532E 02
15	0.00000000E-38	0.00000000E-38	0.00000000E-38	0.00000000E-38	0.00000000E-38	-0.97650666E-01	-0.78536702E 00	0.24742818E 02
16	0.00000000E-38	0.00000000E-38	0.00000000E-38	0.00000000E-38	0.00000000E-38	0.19696419E-01	-0.15841078E 00	0.49906972E 01
17	-0.12423848E 06	0.00000000E-38	0.00000000E-38	0.00000000E-38	0.00000000E-38	0.14171168E-02	-0.11353899E-01	0.35770213E 00
18	0.00000000E-38	0.00000000E-38	0.00000000E-38	0.00000000E-38	0.00000000E-38	-0.47666668E-03	-0.38336481E-02	0.12077825E 00
19	0.00000000E-38	0.00000000E-38	0.00000000E-38	0.00000000E-38	0.00000000E-38	0.18336624E-03	-0.14747447E-02	0.46461511E-01
20	0.00000000E-38	-0.77488372E 06	0.00000000E-38	0.00000000E-38	0.00000000E-38	0.52620942E-04	-0.42321015E-03	0.13333144E-01
21	0.00000000E-38	0.00000000E-38	-0.54289320E 05	0.00000000E-38	0.00000000E-38	0.13650216E-04	-0.10978347E-03	0.34587045E-02
22	0.00000000E-38	0.00000000E-38	0.00000000E-38	0.00000000E-38	0.00000000E-38	0.32694211E-05	-0.26294705E-04	0.82840896E-03
23	0.00000000E-38	0.00000000E-38	0.00000000E-38	-0.54289320E 05	0.00000000E-38	0.98131483E-06	-0.78923401E-05	0.24864645E-03
24	0.00000000E-38	0.00000000E-38	0.00000000E-38	0.00000000E-38	0.00000000E-38	0.55223233E-06	-0.44413207E-05	0.13992285E-03
25	0.00000000E-38	0.00000000E-38	0.00000000E-38	0.00000000E-38	-0.38300240E 07	0.55223233E-06	-0.44132207E-05	0.13992285E-03
26	0.00000000E-38	0.00000000E-38	0.00000000E-38	0.00000000E-38	0.00000000E-38	0.20657710E-06	-0.16614208E-05	0.52342701E-04

TABLE V.- REDUCED STIFFNESS MATRIX FOR 1/40-SCALE SATURN V LAUNCH VEHICLE – Continued

(b) SI Units – Continued

ROW	COL 9	10	11	12	13	14	15	16
1	0.00000000E-38	0.00000000E-38	0.00000000E-38	0.00000000E-38	0.00000000E-38	0.00000000E-38	0.00000000E-38	0.00000000E-38
2	0.00000000E-38	0.00000000E-38	0.00000000E-38	0.00000000E-38	0.00000000E-38	0.00000000E-38	0.00000000E-38	0.00000000E-38
3	0.00000000E-38	0.00000000E-38	0.00000000E-38	0.00000000E-38	0.00000000E-38	0.00000000E-38	0.00000000E-38	0.00000000E-38
4	0.00000000E-38	0.00000000E-38	0.00000000E-38	0.00000000E-38	0.00000000E-38	0.00000000E-38	0.00000000E-38	0.00000000E-38
5	0.00000000E-38	0.00000000E-38	0.00000000E-38	0.27385534E 01	0.36782354E 00	0.59057848E 00	0.29797636E 00	0.97650666E-01
6	-0.21252416E 06	0.69096097E 04	-0.21921951E 03	-0.22025139E 02	-0.29582643E 01	-0.47497973E 01	-0.23965101E 01	-0.78536702E 00
7	0.17092507E 07	-0.55571354E 05	0.17630988E 04	0.69389724E 03	0.93199474E 02	0.14964133E 03	0.75501532E 02	0.24742818E 02
8	-0.60390422E 07	0.17507634E 07	-0.55546046E 05	-0.17623712E 05	-0.23670950E 04	-0.38006143E 04	-0.19175998E 04	-0.62842201E 03
9	0.90831736E 07	-0.59251472E 07	0.14107673E 07	0.64371558E 06	0.86459423E 05	0.29707379E 06	0.70041365E 05	0.49120404E 05
10	-0.59251472E 07	0.85542622E 07	-0.52983395E 07	-0.50412830E 07	-0.64734916E 06	0.14580164E 06	0.14988857E 06	0.63975779E 05
11	0.14107673E 07	-0.52983395E 07	0.82907658E 07	0.95466389E 07	0.18502322E 06	0.38691716E 06	0.19521904E 06	0.21714460E 06
12	-0.17623712E 05	0.70041365E 06	-0.50412830E 07	-0.57925423E 07	-0.57925423E 07	-0.73086324E 07	0.64734916E 06	0.16502174E 07
13	-0.23670950E 04	0.86459423E 05	0.18502322E 06	0.38669171E 06	0.12909012E 08	-0.82926151E 07	0.81833106E 06	-0.25104456E 07
14	-0.38006143E 04	0.13881948E 04	0.29707379E 06	0.19521904E 06	-0.82926151E 07	0.16502174E 08	-0.73086324E 07	0.54683265E 07
15	-0.19175998E 04	0.70041365E 04	0.14988857E 06	0.63975779E 05	0.64734916E 06	-0.73086324E 07	0.25104456E 08	-0.51974262E 07
16	-0.62842201E 03	-0.22953453E 05	0.49120404E 05	0.12904098E 05	0.21214460E 06	0.81833106E 06	-0.25104456E 07	0.11377127E 07
17	-0.12675452E 03	0.46297771E 04	0.99077260E 04	0.92488546E 03	0.42790174E 05	0.33285358E 05	0.51868519E 06	0.38414909E 06
18	-0.90849755E 01	0.33183362E 03	0.71012417E 03	0.31228790E 03	0.30669335E 04	0.23856874E 04	0.37176127E 05	0.14777617E 06
19	-0.30675452E 01	0.11204374E 03	0.23977368E 03	0.12013229E 03	0.10355512E 04	0.80552821E 03	0.12552533E 05	0.42407594E 05
20	-0.11800368E 01	0.43101481E 02	0.92237196E 02	0.34474580E 02	0.39836040E 03	0.30987415E 03	0.48287637E 04	0.11000807E 05
21	-0.33863730E 00	0.12368910E 02	0.26469476E 02	0.89429312E 01	0.11431821E 03	0.88925145E 02	0.13857190E 04	0.26348499E 04
22	-0.87844727E-01	0.32085759E 01	0.68663547E 01	0.21419593E 01	0.29654889E 02	0.23067763E 02	0.35946456E 03	0.79084865E 03
23	-0.21040063E-01	0.76849959E 00	0.16445898E 01	0.64290782E 00	0.71027679E 01	0.55250572E 01	0.86096884E 02	0.25841928E 03
24	-0.63151624E-02	0.23066470E 00	0.49362265E 00	0.36178874E 00	0.21318917E 01	0.16583427E 01	0.25841928E 02	0.14542238E 03
25	-0.35537826E-02	0.12980382E 00	0.27778027E 00	0.24195930E 00	0.11996967E 01	0.93321270E 00	0.14542238E 02	0.44504068E 03
26	-0.13294082E-02	0.48557350E-01	0.10391276E 00	0.13553388E 00	0.44878564E 00	0.34909862E 00	0.54399979E 01	0.16648196E 03

TABLE V.- REDUCED STIFFNESS MATRIX FOR 1/40-SCALE SATURN V LAUNCH VEHICLE – Continued

(b) SI Units – Continued

ROW	COL 17	18	19	20	21	22	23	24
1	-0.12423848E 06	0.00000000E-38	0.00000000E-38	0.00000000E-38	0.00000000E-38	0.00000000E-38	0.00000000E-38	0.00000000E-38
2	0.00000000E-38	0.00000000E-38	0.00000000E-38	-0.77488372E 06	0.00000000E-38	0.00000000E-38	0.00000000E-38	0.00000000E-38
3	0.00000000E-38	0.00000000E-38	0.00000000E-38	0.00000000E-38	-0.54289320E 05	0.00000000E-38	0.00000000E-38	0.00000000E-38
4	0.00000000E-38	0.00000000E-38	0.00000000E-38	0.00000000E-38	0.00000000E-38	0.00000000E-38	-0.54289320E 05	0.00000000E-38
5	0.00000000E-38	0.00000000E-38	0.00000000E-38	0.00000000E-38	0.00000000E-38	0.00000000E-38	0.00000000E-38	0.00000000E-38
6	0.19696419E-01	0.14117168E-02	0.47666668E-03	0.18336624E-03	0.52609942E-04	0.13650216E-04	0.32694211E-05	0.98131483E-06
7	-0.15841078E 00	-0.11353899E-01	-0.38336481E-02	-0.14744747E-02	-0.42321015E-03	-0.10978347E-03	-0.26294705E-04	-0.78923401E-05
8	0.49906972E 01	0.35770213E 00	0.12077825E 00	0.46461511E-01	0.13333144E-01	0.34587045E-02	0.82840896E-03	0.24864645E-03
9	-0.12675452E 03	-0.90849755E 01	-0.30675452E 01	-0.11800368E 01	-0.33863730E 00	-0.87844727E-01	-0.21040063E-01	-0.63151624E-02
10	0.46297771E 04	0.33183362E 03	0.11204374E 03	0.43101481E 02	0.12368910E 02	0.32085759E 01	0.76849959E 00	0.23066470E 00
11	0.99077260E 04	0.71012417E 03	0.23977368E 03	0.92237196E 02	0.26469476E 02	0.68663547E 01	0.16445898E 01	0.49362265E 00
12	-0.12904098E 05	0.92485446E 03	0.31228790E 03	0.12013229E 03	0.34474580E 02	0.89429312E 01	0.21419593E 01	0.64290782E 00
13	0.42790174E 05	0.30669335E 04	0.10355512E 04	0.39836040E 03	0.11431821E 03	0.29654889E 02	0.71027679E 01	0.21318917E 01
14	0.33285358E 05	0.23856874E 04	0.80552821E 03	0.30987415E 03	0.88925145E 02	0.23067763E 02	0.55205572E 01	0.16583427E 01
15	0.51865519E 06	0.37176127E 05	0.12552533E 05	0.48287637E 04	0.13857190E 04	0.35946456E 03	0.86096884E 02	0.25841928E 02
16	-0.51974262E 07	0.11377127E 07	0.38414909E 06	0.14777617E 06	0.42407594E 05	0.11000807E 05	0.26348499E 04	0.79084865E 03
17	0.13731106E 08	-0.11400527E 08	0.15445451E 07	0.59416246E 06	0.17050787E 06	0.44230857E 05	0.10593920E 05	0.31797588E 04
18	-0.11400527E 08	0.24972836E 08	-0.18284038E 08	0.25435400E 07	0.72992425E 06	0.18934713E 06	0.45351331E 05	0.13612175E 05
19	0.15445451E 07	-0.18284038E 08	0.32126285E 08	-0.19381465E 08	0.26619776E 07	0.69053440E 06	0.16539283E 06	0.49642560E 05
20	0.59416246E 06	0.25435400E 07	-0.19381465E 08	0.35545730E 08	-0.23784807E 08	0.37756663E 07	0.90432587E 06	0.27143288E 06
21	0.17050787E 06	0.72992425E 06	0.26619776E 07	-0.23784807E 08	0.44930725E 08	-0.29667328E 08	0.33826057E 07	0.10152871E 07
22	0.44230857E 05	0.18934713E 06	0.69053440E 06	0.37756663E 07	-0.29667328E 08	0.49664937E 08	-0.29377224E 08	-0.29873338E 07
23	0.10593920E 05	0.45351331E 05	0.16539283E 06	0.90432587E 06	0.33826057E 07	-0.29377224E 08	0.84507697E 08	-0.63615331E 08
24	0.31797588E 04	0.13612175E 05	0.49642560E 05	0.27143288E 06	0.10152871E 07	0.29873338E 07	-0.63615331E 08	0.11347712E 09
25	0.17893715E 04	0.76609000E 04	0.27935759E 05	0.15274562E 06	0.57134070E 06	0.16810864E 07	0.40282018E 07	-0.52073074E 08
26	0.66937269E 03	0.28655062E 04	0.10450281E 05	0.57139474E 05	0.21372861E 06	0.62886514E 06	0.15068801E 07	0.52792416E 07

40

TABLE V.- REDUCED STIFFNESS MATRIX FOR 1/40-SCALE SATURN V LAUNCH VEHICLE – Concluded

(b) SI Units – Concluded

ROW	COL 25	26
1	0.00000000E-38	0.00000000E-38
2	0.00000000E-38	0.00000000E-38
3	0.00000000E-38	0.00000000E-38
4	0.00000000E-38	0.00000000E-38
5	-0.38300240E 07	0.00000000E-38
6	0.55222323E-06	0.20657710E-06
7	-0.44413207E-05	-0.16614208E-05
8	0.13992285E-03	0.52342701E-04
9	-0.35537826E-02	-0.13294082E-02
10	0.12980382E 00	0.48557350E-01
11	0.27778027E 00	0.10391276E 00
12	0.36178874E 00	0.13533887E 00
13	0.11996967E 01	0.44878564E 00
14	0.93321270E 00	0.34909862E 00
15	0.14542238E 02	0.54399979E 01
16	0.44504068E 03	0.16664196E 03
17	0.17893715E 04	0.66937269E 03
18	0.76600900E 04	0.28655062E 04
19	0.27935759E 05	0.10450281E 05
20	0.15274562E 06	0.57139474E 05
21	0.57134070E 06	0.21372861E 06
22	0.16810864E 07	0.62886514E 06
23	0.40282018E 07	0.15068801E 07
24	-0.52073074E 08	0.52792416E 07
25	0.49431884E 08	-0.77000135E 07
26	-0.77000135E 07	0.21506146E 07

TABLE VI.- MASS ASSIGNED TO NODES OF UMBILICAL TOWER

Node	Nodal mass	
	lbf-sec^2/in.	kg
1, 2, 3, 4	0.01057	1.85109
9, 10, 11, 12	.00097	.16987
17, 18, 19, 20	.003975	.69613
25, 26, 27, 28	.001095	.19176
33, 34, 35, 36	.001265	.22154
41, 42, 43, 44	.009875	1.72938
49, 50, 51, 52	.001585	.27758
57, 58, 59, 60	.001895	.33187
65, 66, 67, 68	.001893	.33152
73, 74, 75, 76	.002485	.43519
81, 82, 83, 84	.002780	.48685
89, 90, 91, 92	.02830	4.95609
97, 98, 99, 100	.003355	.58755
105, 106, 107, 108	.003750	.65673
113, 114, 115, 116	.01320	2.31167
121, 122, 123, 124	.00695	1.21713
129, 131, 133, 135	.02090	3.66015
141, 143, 145, 147	.0084	1.47107
153, 154, 155, 156	.003155	.55253

TABLE VII.- MASS ASSIGNED TO NODES OF LAUNCH PLATFORM

Node	Nodal mass	
	lbf-sec^2/in.	kg
1	0.01213	2.12429
2	.01734	3.03670
3	.01374	2.40624
4	.01373	2.40449
5	.01889	3.30815
6	.03501	6.13119
7	.01213	2.12429
8	.03030	5.30634
9	.01988	3.48152
10	.02750	4.81599
11	.02001	3.50429
12	.02400	4.20304
13	.01989	3.48327
14	.02930	5.13122
15	.04418	7.73710
16	.02292	4.01391
17	.02563	4.48850
18	.02926	5.12421
19	.00305	.53414
20	.00225	.39404
21	.05104	8.93848
22	.02518	4.40969
23	.00305	.53414
24	.05336	9.34477
25	.02638	4.61985
26	.02628	4.60233
27	.00305	.53414
28	.03844	6.73188
29	.02272	3.97888
30	.03518	6.16096
31	.03305	5.78794
32	.01575	2.75825
33	.04044	7.08213
34	.00225	.39404
35	.00225	.39404
36	.03844	6.73188
37	.01788	3.13127
38	.02645	4.63210
39	.02645	4.63210
40	.00305	.53414
41	.00213	.37302
42	.00305	.53414
43	.00305	.53414

TABLE VIII.- MASS ASSIGNED TO NODES OF SATURN V MODEL

Node	Nodal mass	
	$lbf\text{-}sec^2/in.$	kg
1	0.000482	0.084411
2	.002419	.423632
3	.051489	9.017106
4	.051036	8.937773
5	.014549	2.547920
6	.00008	.014010
7	.000161	.028195
8	.000161	.028195
9	.000161	.028195
10	.000161	.028195
11	.000743	.130119
12	.002803	.490881
13	.004451	.779490
14	.002938	.514523
15	.003264	.571614
16	.005614	.983162
17	.035469	6.211574
18	.010611	1.858271
19	.03544	6.206495
20	.096603	16.917778
21	.127199	22.275959
22	.1947	34.097196
23	.026832	4.699003
24	.142015	24.870638
25	.009165	1.605037

TABLE IX.- FREQUENCIES FOR VARIOUS CONFIGURATIONS

[Experimental frequencies are obtained from refs. 6 and 7]

Mode	Vehicle alone			Tower alone, x-direction			Tower alone, y-direction			Tower mounted on platform / No vehicle			Tower and vehicle mounted on platform				
													Vehicle with spring restraint			Vehicle cantilevered to plot form	
	f_a, Hz	f_e, Hz	Difference, percent (a)	f_a, Hz	f_e, Hz	Difference, percent (a)	f_a, Hz	f_e, Hz	Difference, percent (a)	f_a, Hz	f_e, Hz	Difference, percent (a)	f_a, Hz	f_e, Hz	Difference, percent (a)	f_a, Hz	Difference, percent (a)
1st vehicle bending	10.52	10.9	-3.5										9.75	9.5	+2.6	11.61	+22.0
1st vehicle bending and slosh	13.18	12.9	+2.2										13.0	12.9	+0.77	13.95	+8.1
1st tower				32.37	b28.2 b29.8	---	26.11	b28.2 b29.8	---	32.29	b27.5	---	32.29	b28.4	---	32.29	---
2d vehicle bending	36.13	34.7	+4.1										35.15	34.9	+0.72	38.38	+10.0
3d vehicle bending	68.54	63.2	+8.5										67.27	61.9	+8.4	70.56	+14.0
Coupled 3d vehicle bending and 2d tower													75.43	68.1	+11.0	75.51	+11.0
2d tower				76.59	77.1	-0.66	93.67	95.0	-1.4	75.4	67.48	+12.0					
4th vehicle bending	114.7	95.7	+20.0										113.4	98.1	+16.0	115.4	+17.0
Coupled 5th vehicle bending and 3d tower													130.7	111.9	+17.0	130.7	+17.0
5th vehicle bending	138.8	127.0	+8.8														
3d tower				133.5	139.1	-3.6	180.9	173.8	+4.0	131.2	142.7	-8.0					
4th tower				202.4	214.0	-5.4	249.2	227.1	+9.7	205.5	215.1	-4.5					
5th tower				275.5	269.0	+2.4	279.2	273.3	+2.2								

aPercent difference = $\dfrac{f_a - f_e}{f_e} \times 100$.

bSignificant out-of-plane motion observed experimentally.

45
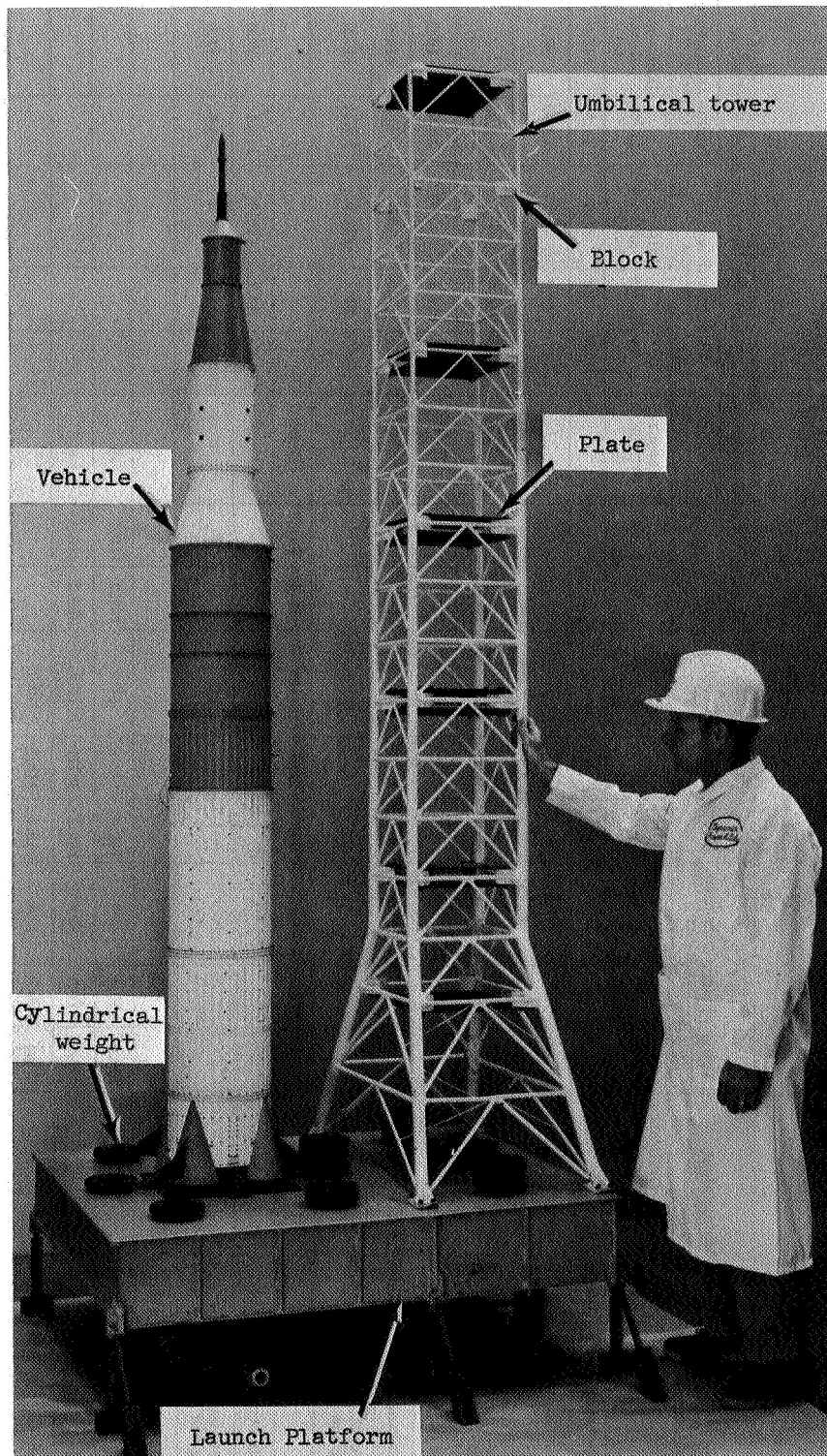
Figure 1.- 1/40-scale dynamic model of the Apollo-Saturn V – umbilical tower configuration.   L-64-8911.1
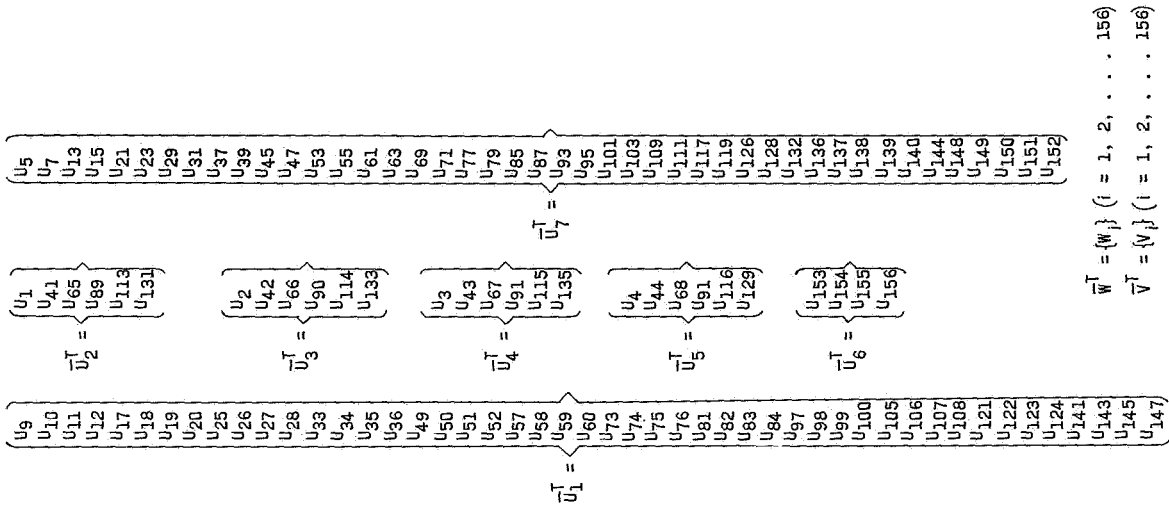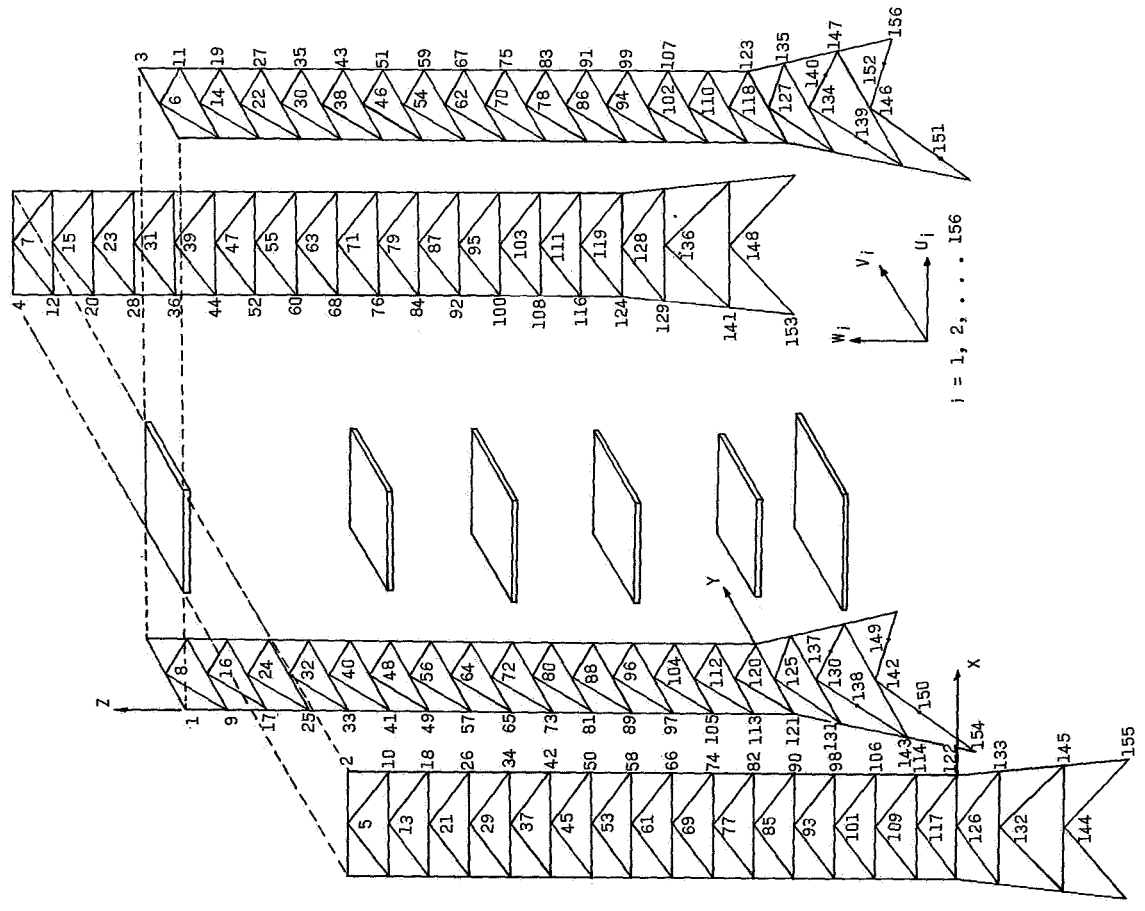
Figure 2.- Idealization of umbilical tower.

47
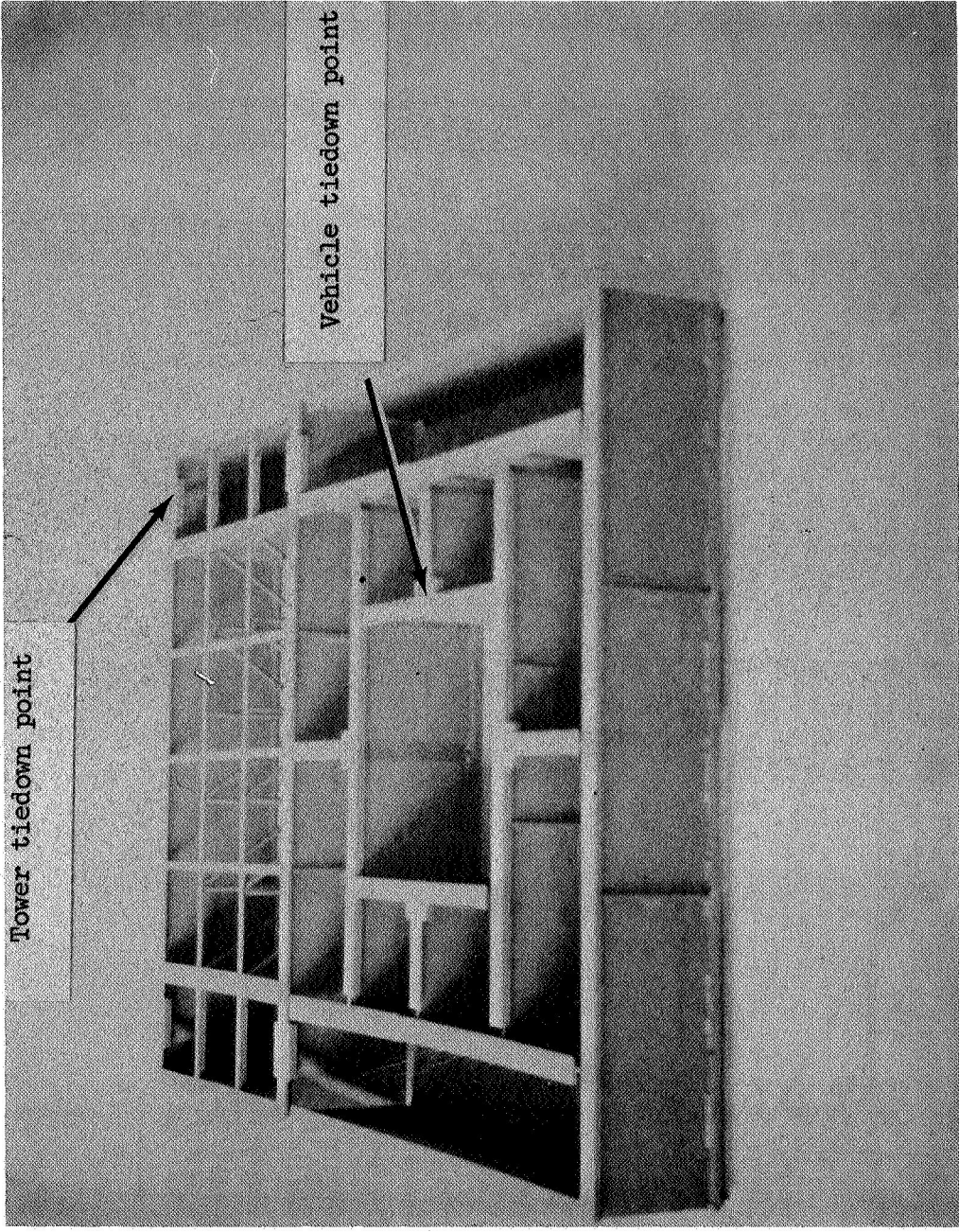
Figure 3.- Launch-platform construction.

L-68-5625

48

Figure 4.- Idealization of launch platform.

49
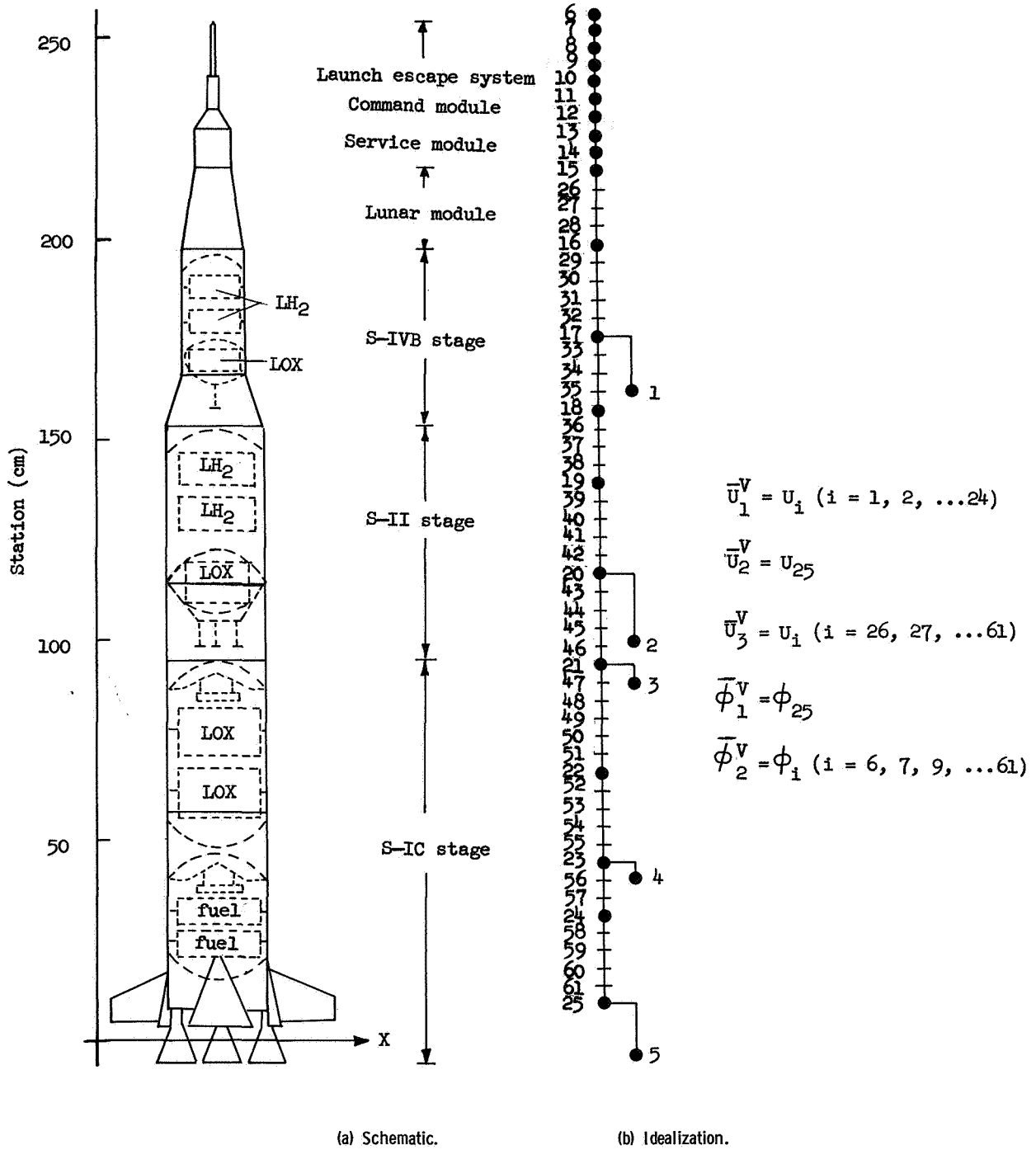
Figure 5.- Schematic and idealization of Apollo-Saturn V launch vehicle.

$$\overline{U}_1^V = U_i \quad (i = 1, 2, \ldots 24)$$

$$\overline{U}_2^V = U_{25}$$

$$\overline{U}_3^V = U_i \quad (i = 26, 27, \ldots 61)$$

$$\overline{\phi}_1^V = \phi_{25}$$

$$\overline{\phi}_2^V = \phi_i \quad (i = 6, 7, 9, \ldots 61)$$

(a) Schematic.   (b) Idealization.

$$\bar{s}_1 = U_i \ (i = 25, \ 26, \ \ldots \ 72)$$

$$\bar{s}_2 = U_i \ (i = 73, \ 74, \ \ldots \ 78)$$

$$\bar{s}_3 = \text{Defined on figure}$$

$$\bar{s}_4 = W_i \ (i = 79, \ 80, \ \ldots \ 108)$$

$$\bar{s}_5 = \phi_{109}$$

$$\bar{s}_6 = \phi_{110}$$

$$\bar{s}_7 = U_i \ (i = 1, \ 2, \ \ldots 24)$$
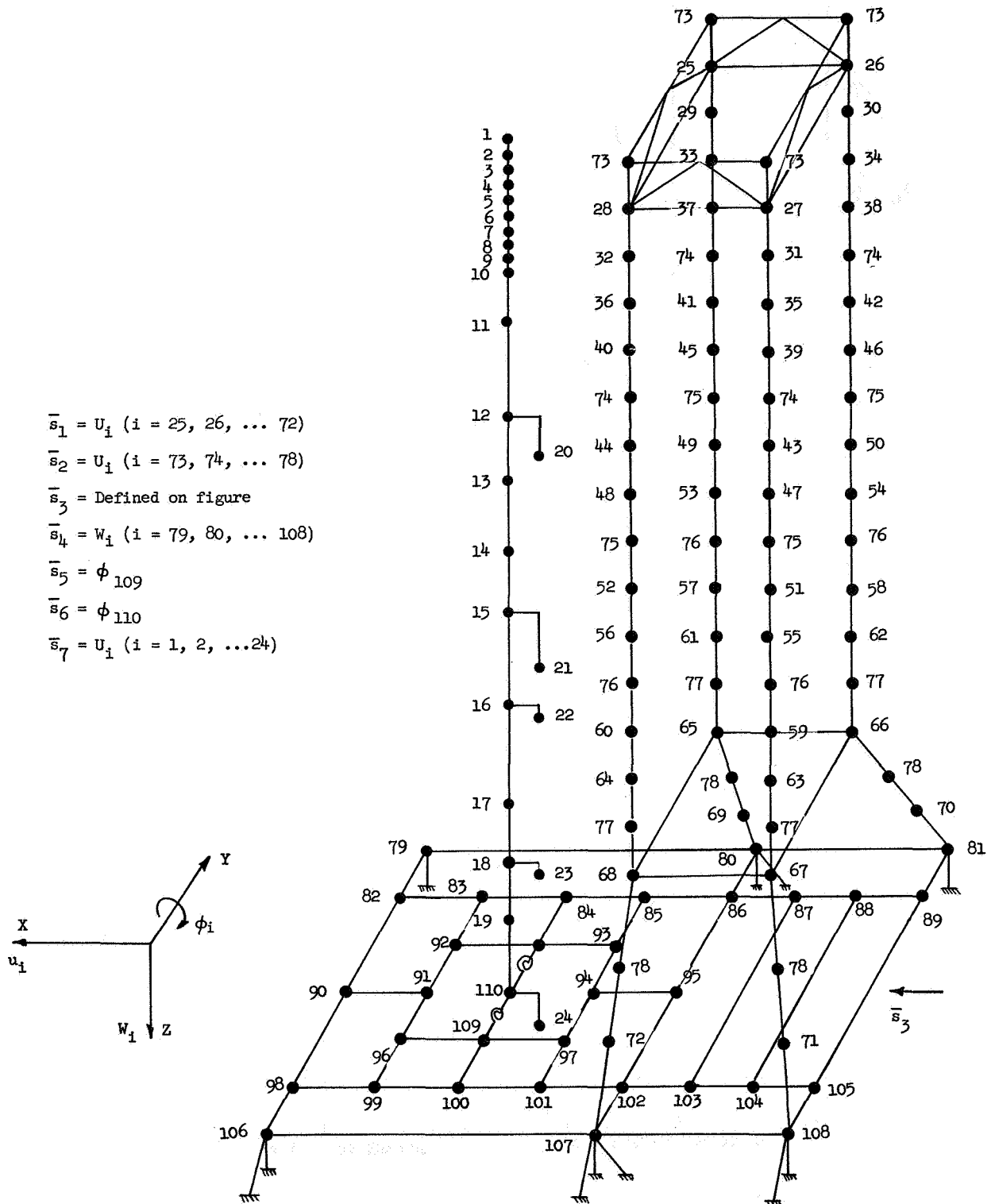
Figure 6.- Idealization of complete Apollo-Saturn V—umbilical-tower configuration.
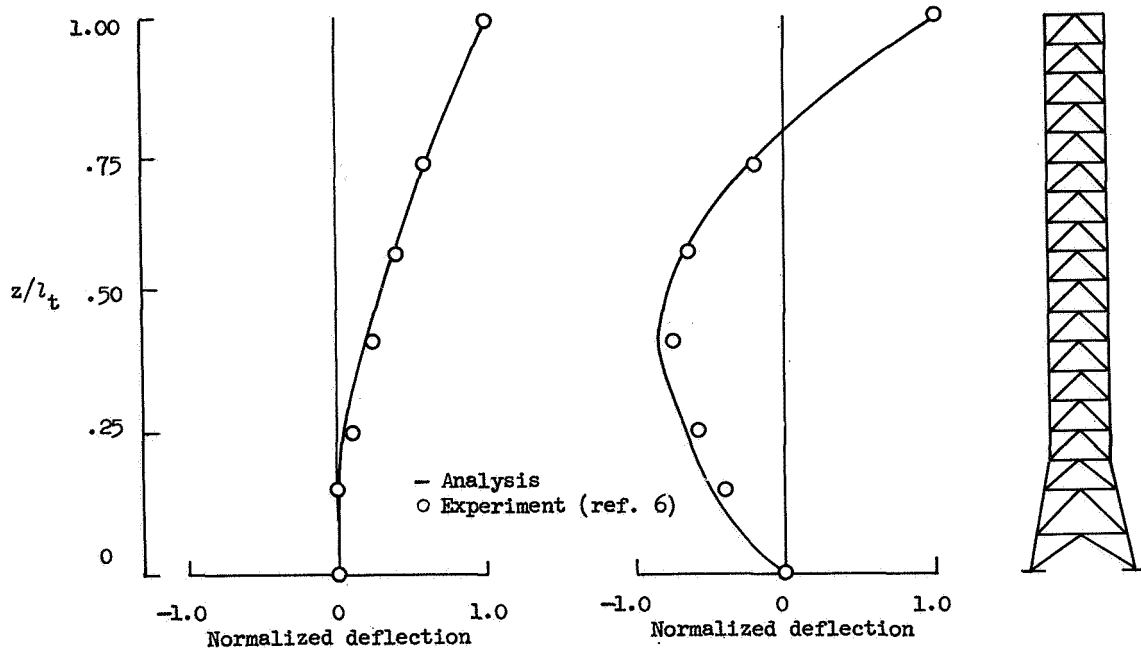
(a) First mode; f_a = 32.37 Hz; f_e = 29.8 Hz.

(b) Second mode; f_a = 76.59 Hz; f_e = 77.1 Hz.
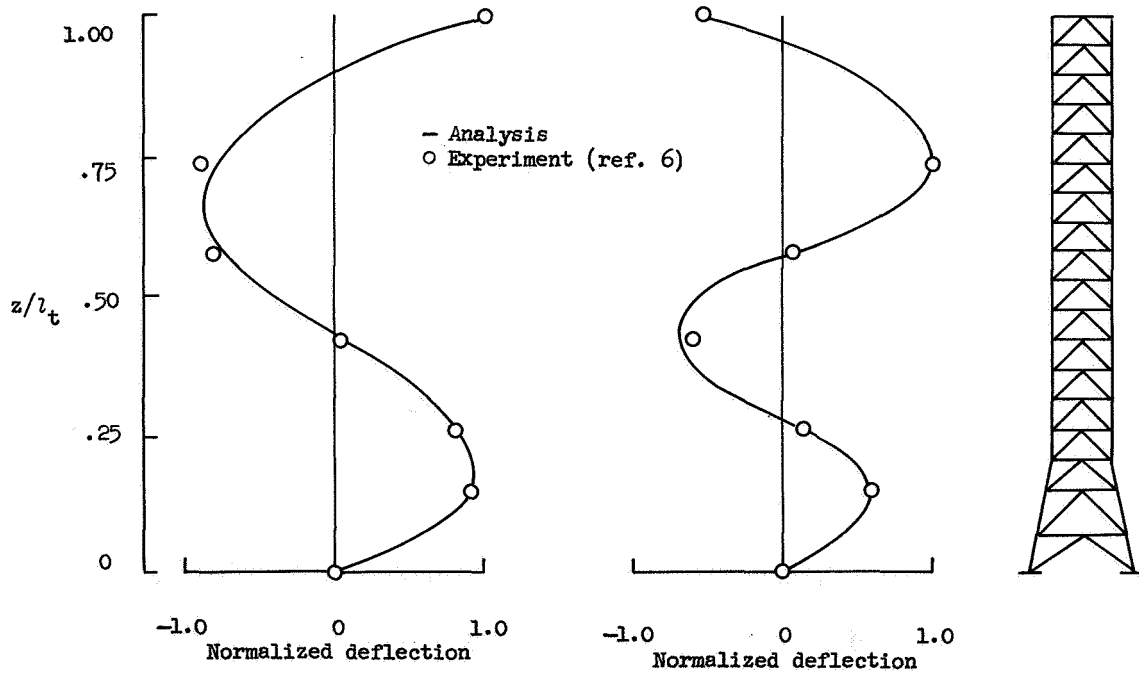
(c) Third mode; f_a = 133.5 Hz; f_e = 139.1 Hz.

(d) Fourth mode; f_a = 202.4 Hz; f_e = 214.0 Hz.

Figure 7.- Natural modes of 1/40-scale Saturn V umbilical tower fixed to rigid foundation.
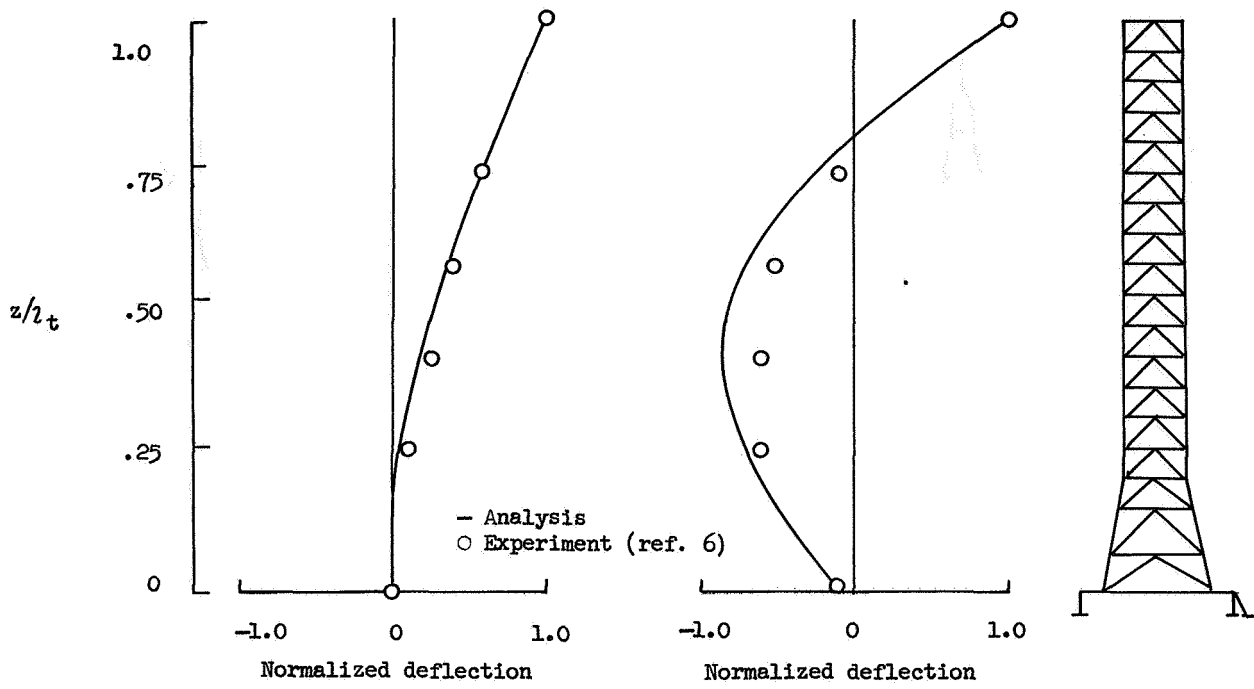
(a) First mode; $f_a = 32.29$ Hz; $f_e = 27.5$ Hz.

(b) Second mode; $f_a = 75.40$ Hz; $f_e = 67.48$ Hz.
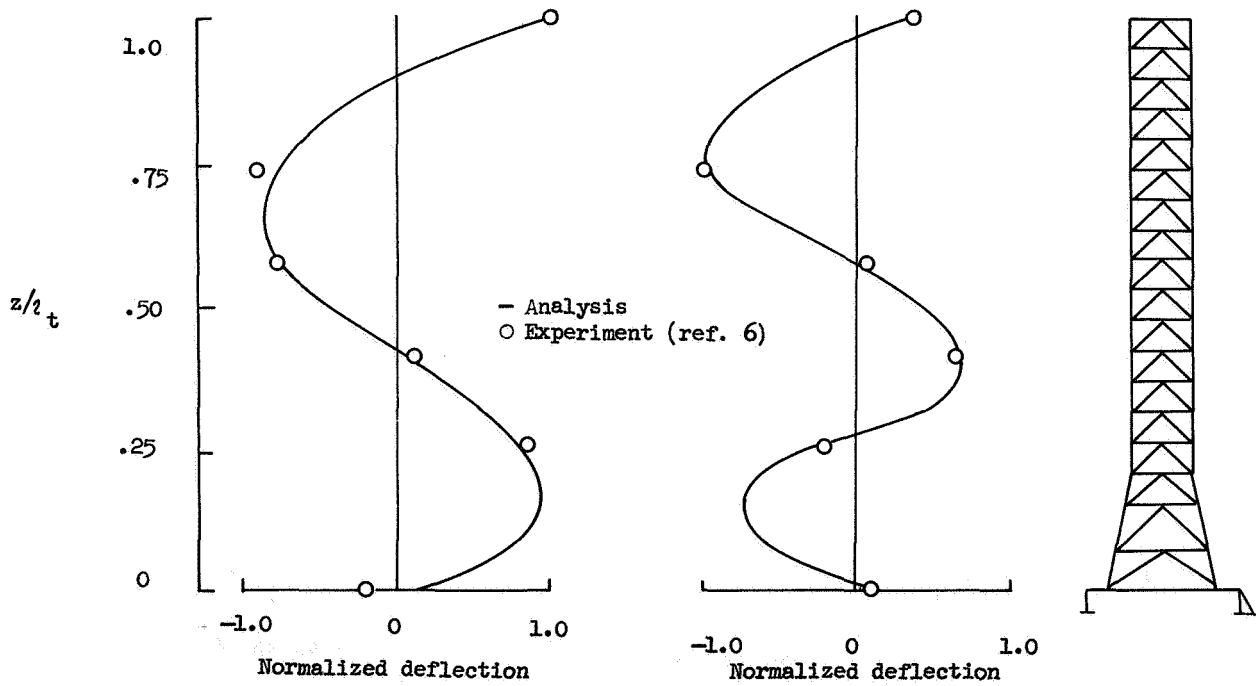
(c) Third mode; $f_a = 131.2$ Hz; $f_e = 142.7$ Hz.

(d) Fourth mode; $f_a = 205.5$ Hz; $f_e = 215.7$ Hz.

Figure 8.- Natural modes at 1/40-scale Saturn V umbilical tower mounted on the launch platform.

(a) First mode; f_a = 10.52 Hz; f_e = 10.9 Hz.

(b) Second mode; f_a = 36.13 Hz; f_e = 34.7 Hz.

(c) Third mode; f_a = 68.54 Hz; f_e = 63.2 Hz.

(d) Fourth mode; f_a = 114.7 Hz; f_e = 95.7 Hz.
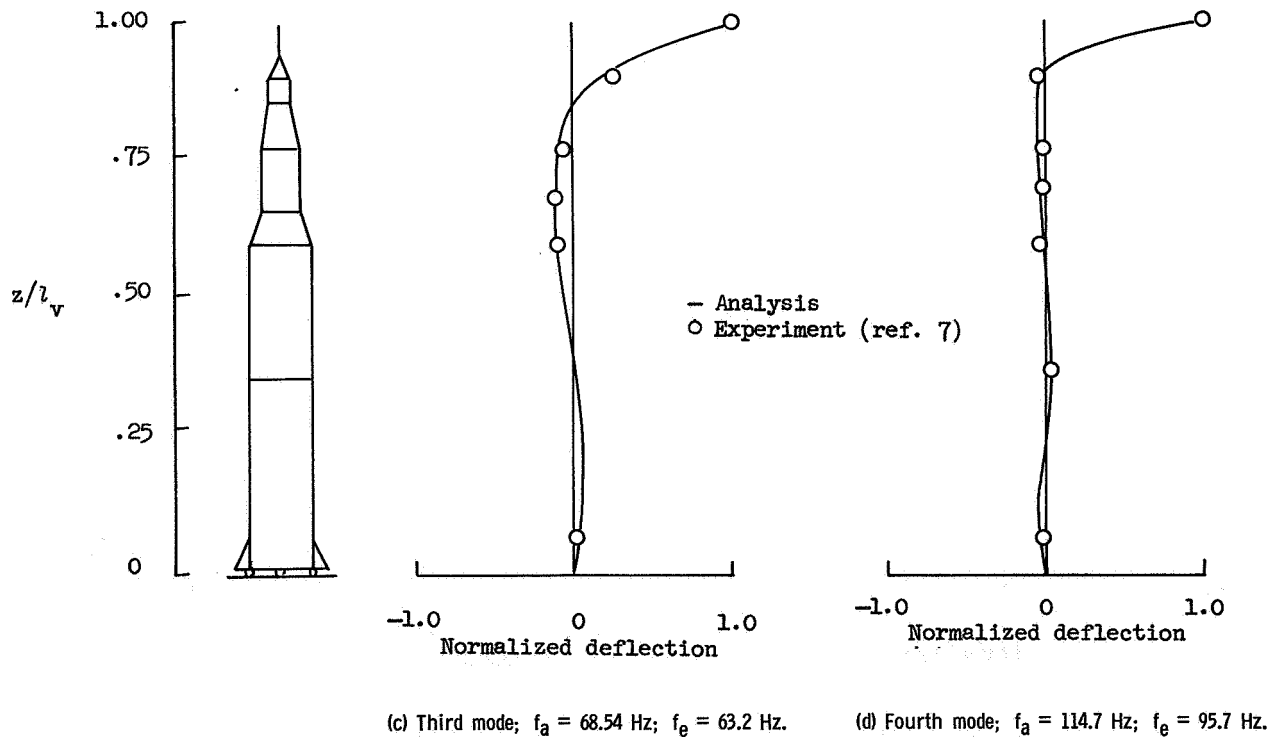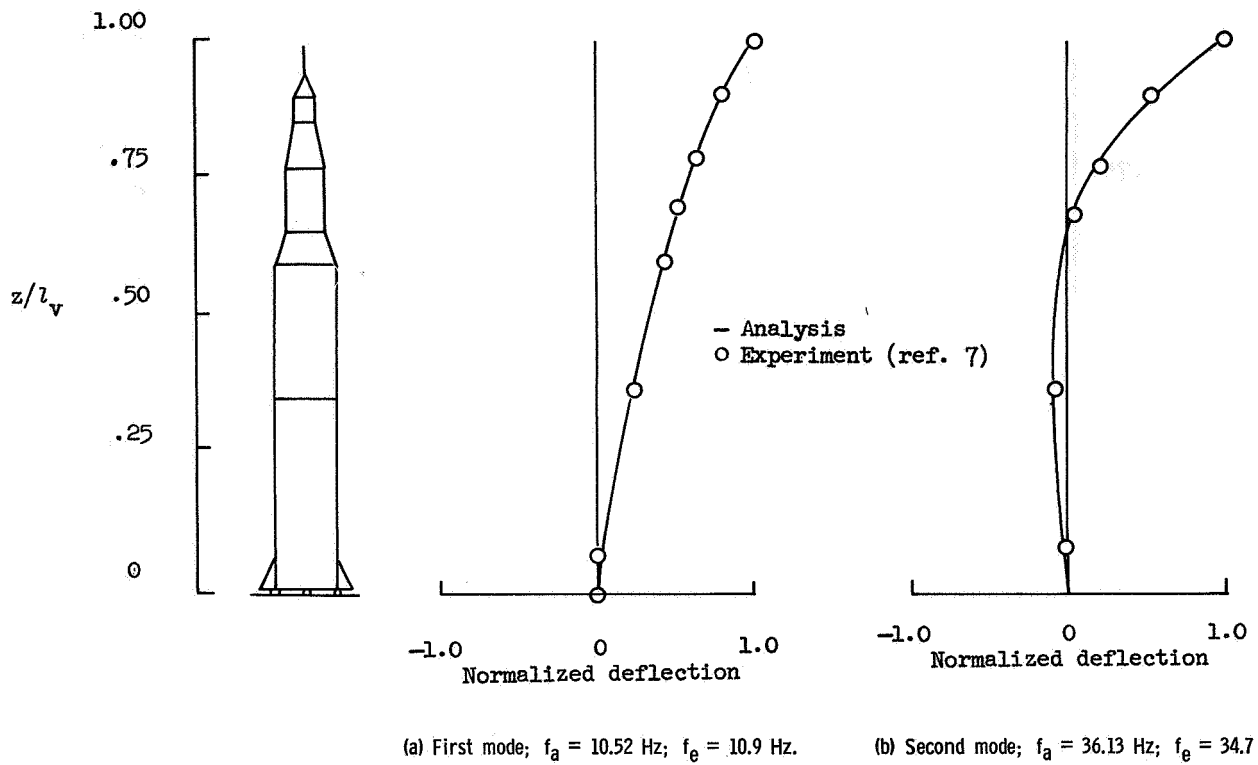
Figure 9.- Natural modes of 1/40-scale Apollo-Saturn V launch vehicle fixed to a rigid foundation.
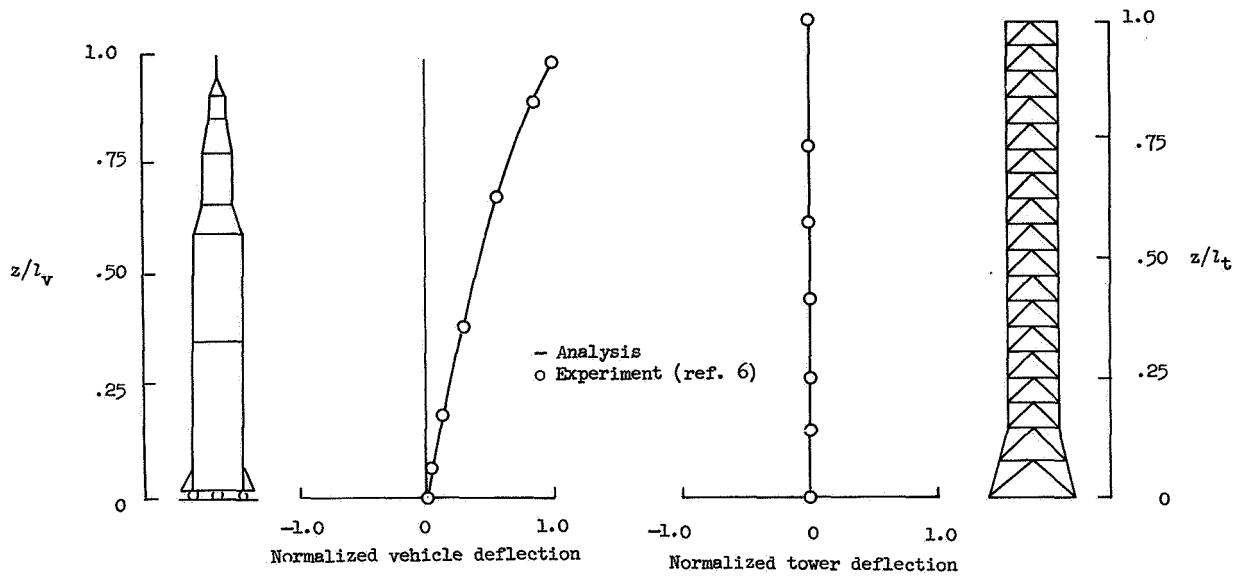
(a) First mode; $f_a = 9.75$ Hz; $f_e = 9.50$ Hz.
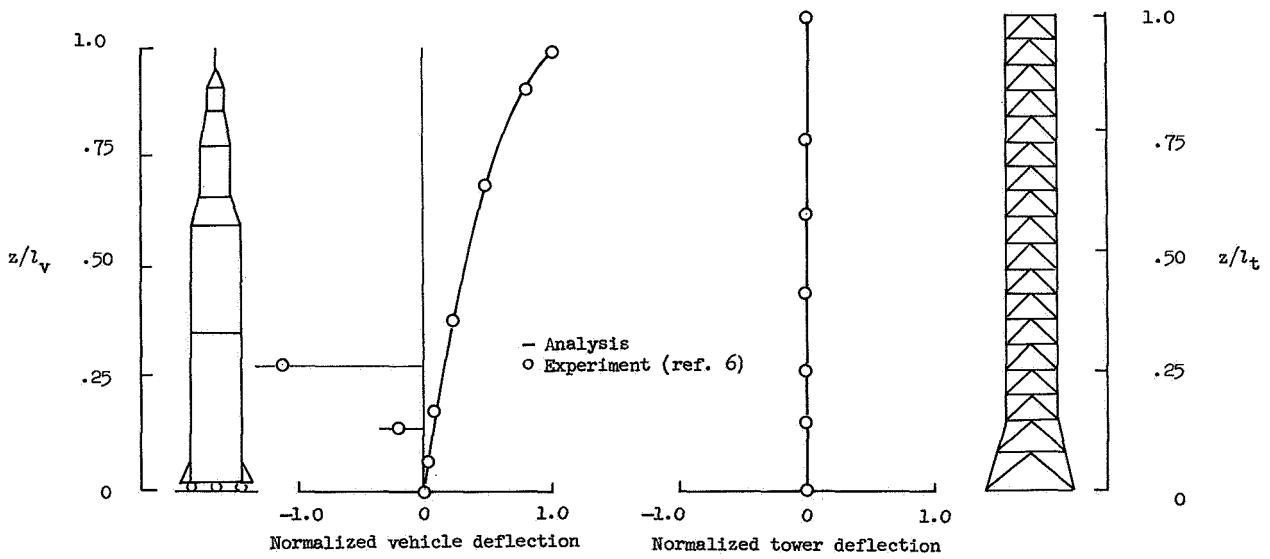
(b) Second mode; $f_a = 13.0$ Hz; $f_e = 12.9$ Hz.

Figure 10.- Natural modes of 1/40-scale Apollo Saturn V vehicle-umbilical tower configuration. First stage, 85 percent full; all other stages, 100 percent full.
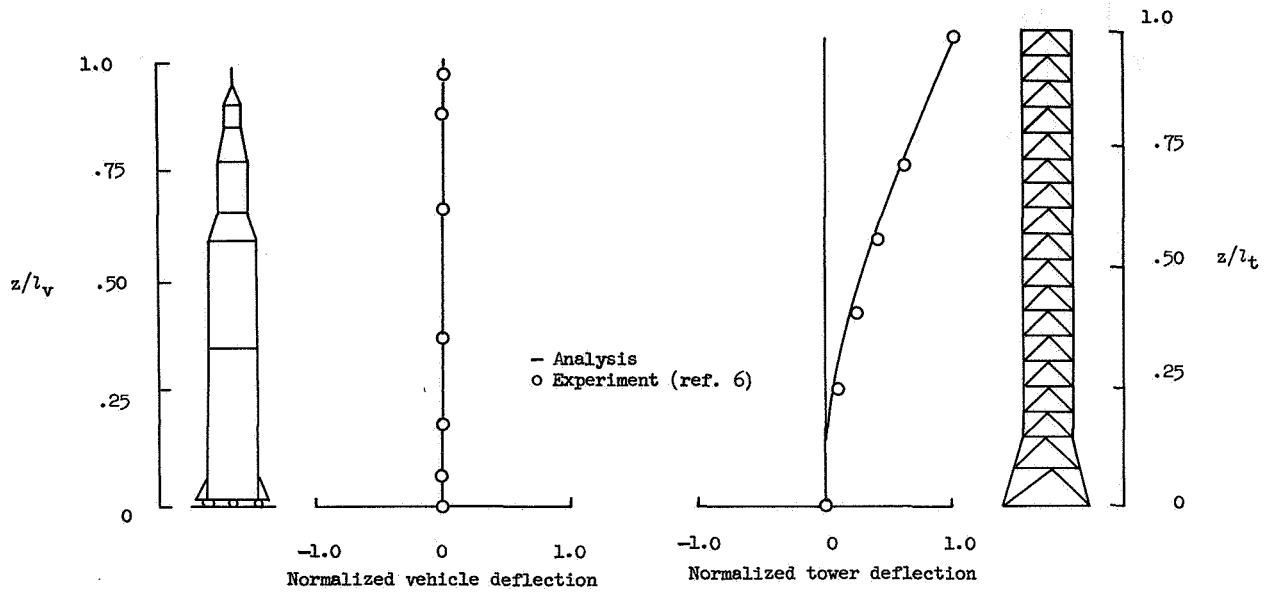
(c) Third mode; $f_a = 32.29$ Hz; $f_e = 28.4$ Hz.
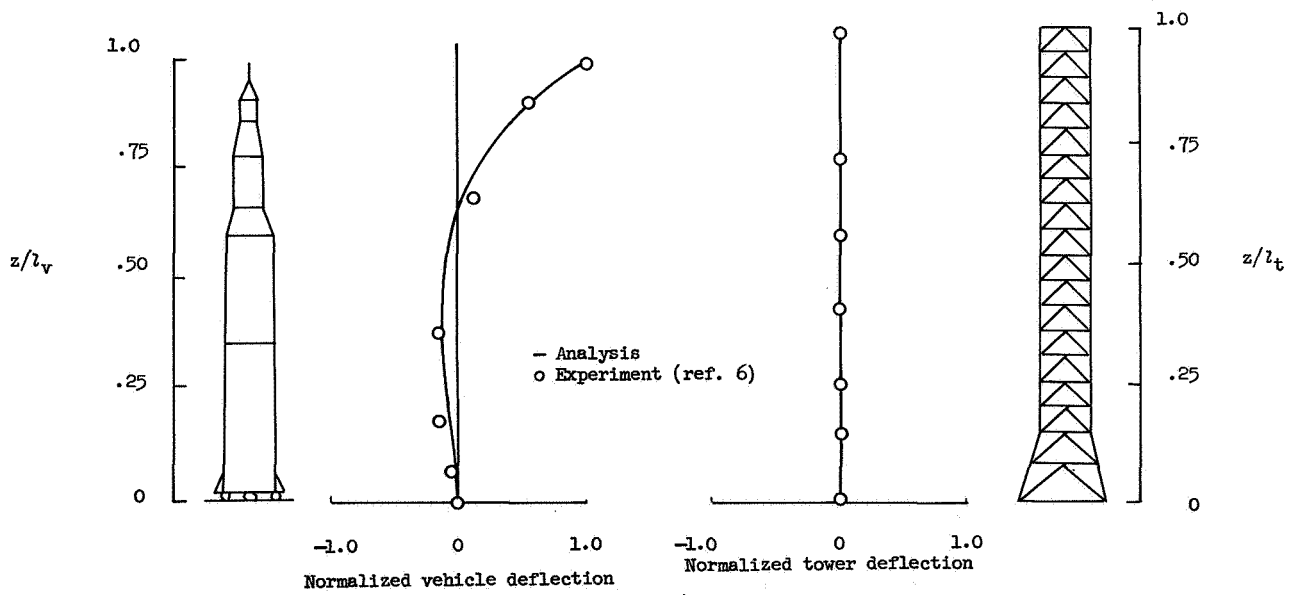
(d) Fourth mode; $f_a = 35.15$ Hz; $f_e = 34.9$ Hz.

Figure 10.- Continued.

56
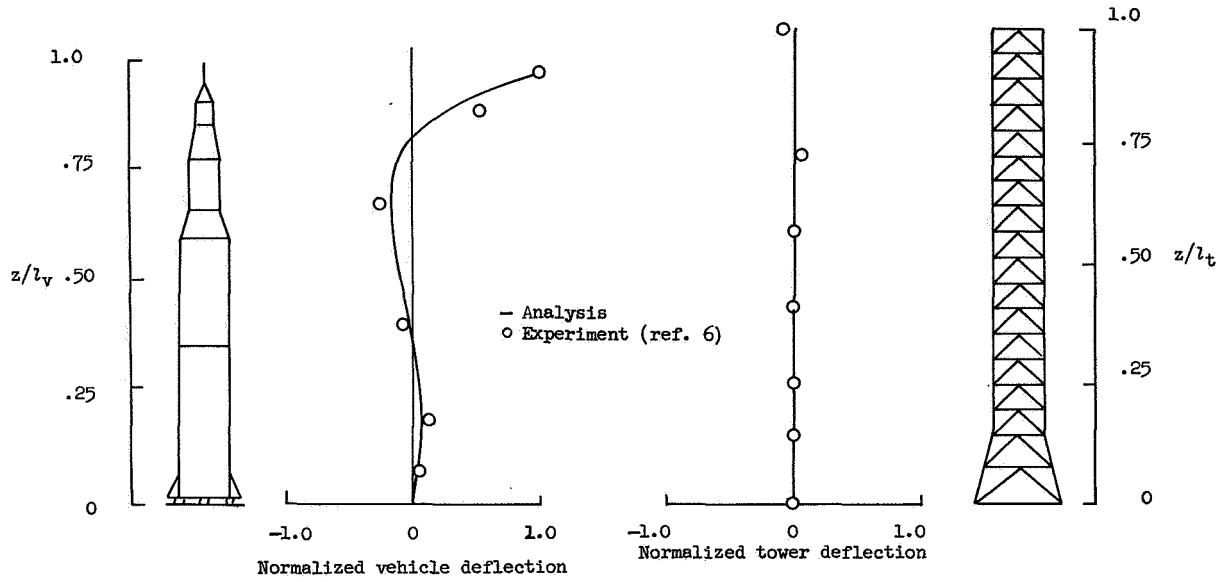
(e) Fifth mode; f_a = 67.27 Hz; f_e = 61.9 Hz.
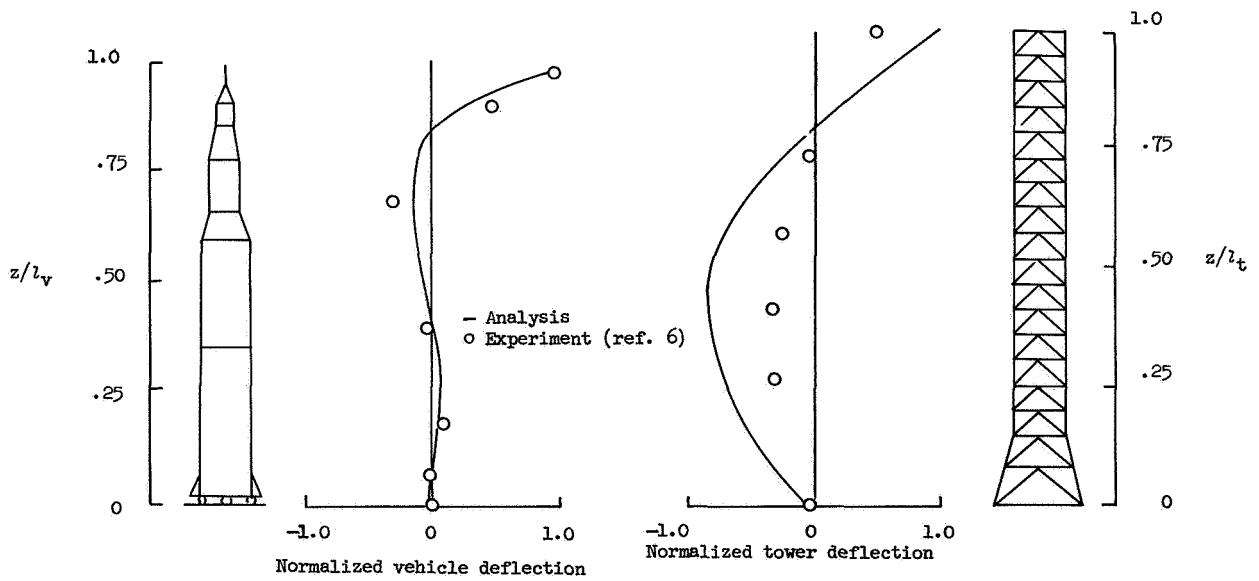
(f) Sixth mode; f_a = 75.43 Hz; f_e = 68.1 Hz.

Figure 10.- Continued.
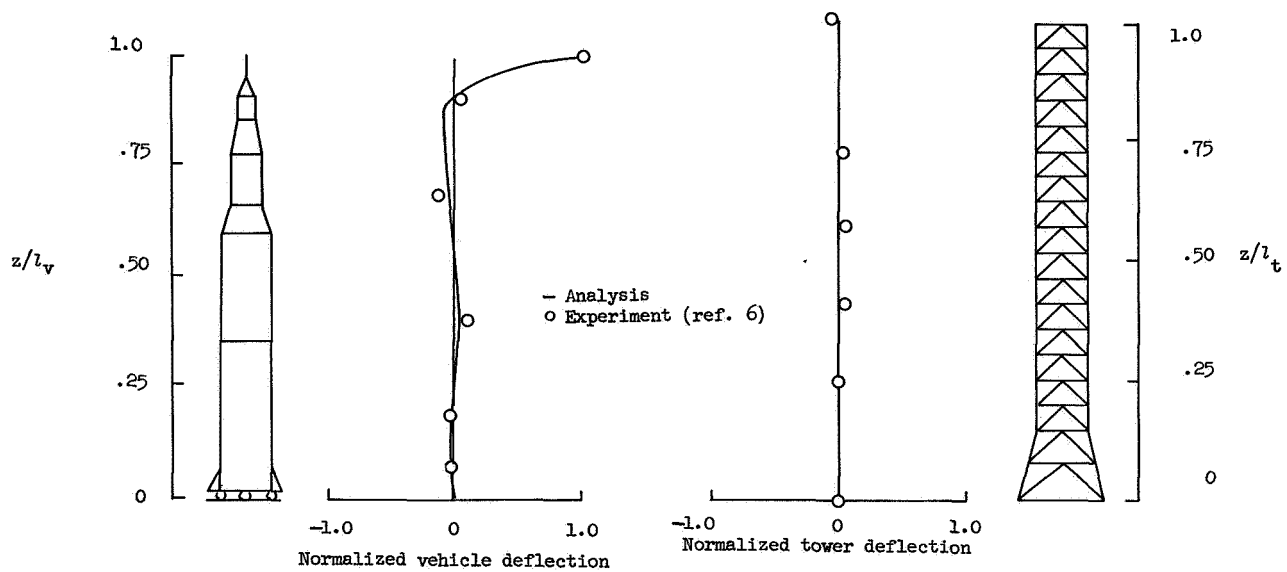
(g) Seventh mode; $f_a = 113.4$ Hz; $f_e = 98.1$ Hz.
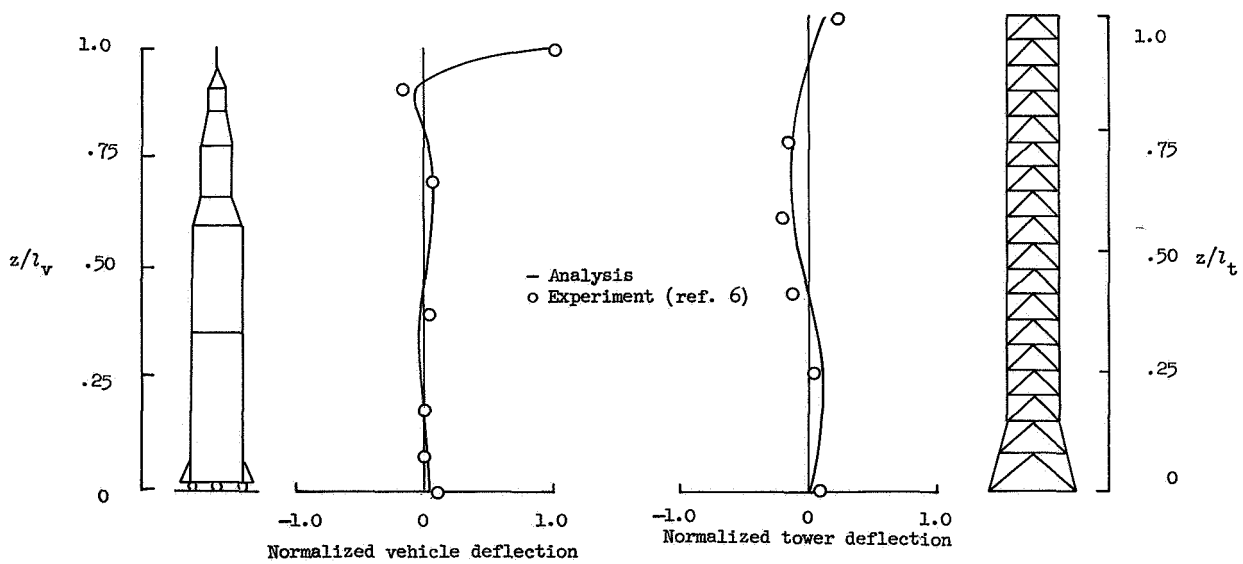
(h) Eighth mode; $f_a = 130.7$ Hz; $f_e = 114.6$ Hz.

Figure 10.- Concluded.

"The aeronautical and space activities of the United States shall be conducted so as to contribute . . . to the expansion of human knowledge of phenomena in the atmosphere and space. The Administration shall provide for the widest practicable and appropriate dissemination of information concerning its activities and the results thereof."

— NATIONAL AERONAUTICS AND SPACE ACT OF 1958

NASA SCIENTIFIC AND TECHNICAL PUBLICATIONS

TECHNICAL REPORTS: Scientific and technical information considered important, complete, and a lasting contribution to existing knowledge.

TECHNICAL NOTES: Information less broad in scope but nevertheless of importance as a contribution to existing knowledge.

TECHNICAL MEMORANDUMS: Information receiving limited distribution because of preliminary data, security classification, or other reasons.

CONTRACTOR REPORTS: Scientific and technical information generated under a NASA contract or grant and considered an important contribution to existing knowledge.

TECHNICAL TRANSLATIONS: Information published in a foreign language considered to merit NASA distribution in English.

SPECIAL PUBLICATIONS: Information derived from or of value to NASA activities. Publications include conference proceedings, monographs, data compilations, handbooks, sourcebooks, and special bibliographies.

TECHNOLOGY UTILIZATION PUBLICATIONS: Information on technology used by NASA that may be of particular interest in commercial and other non-aerospace applications. Publications include Tech Briefs, Technology Utilization Reports and Notes, and Technology Surveys.

Details on the availability of these publications may be obtained from:

SCIENTIFIC AND TECHNICAL INFORMATION DIVISION

NATIONAL AERONAUTICS AND SPACE ADMINISTRATION

Washington, D.C. 20546